The Structure of a Continental Intraplate Volcanic System and Controls from Shear Zones

Insights into the central Hoggar Cenozoic volcanic province, Northwest Africa, from electrical resistivity images

Boukhalfa, Zakaria; Benhallou, Amel Z.; Comeau, Matthew J.; Bouzid, Abderrezak; Bendaoud, Abderrahmane; Deramchi, Aboubakr

DOI
10.1016/j.gr.2024.08.003

Publication date
2024

Document Version
Final published version

Published in
Gondwana Research

Gondwana Research 135 (2024) 133–150

Contents lists available at ScienceDirect

Gondwana Research

journal homepage: www.elsevier.com/locate/gr

The structure of a continental intraplate volcanic system and controls from shear zones: Insights into the central Hoggar Cenozoic volcanic province, Northwest Africa, from electrical resistivity images

Zakaria Boukhalfa [a,b], Amel Z. Benhallou [a], Matthew J. Comeau [c,*], Abderrezak Bouzid [a], Abderrahmane Bendaoud [b], Aboubakr Deramchi [a]

[a] Centre de Recherche en Astonomie, Astrophysique et Géophysique (CRAAG), BP 63, Route de l'Observatoire, Bouzereah, Algiers 16340, Algeria
[b] Faculté des Sciences de la Terre, de Géographie et de l'Aménagement du Territoire, Université des Sciences et Technologie Houari Boumedien (USTHB), Algiers, Algeria
[c] Delft University of Technology, Department of Geoscience and Engineering, Stevinweg 1, 2628 CN Delft, the Netherlands

ARTICLE INFO

Article history:
Received 13 February 2024
Revised 6 June 2024
Accepted 7 August 2024
Available online 13 August 2024
Handling Editor: A. Vasanthi

Keywords:
Intraplate Volcanism
Magnetotelluric
Metasomatism
Melt
Mantle Upwelling

ABSTRACT

Continental intraplate volcanic systems, with their locations far from plate tectonic boundaries, are not well understood: the crustal and lithospheric mantle structure of these systems remain enigmatic and there is no consensus on the mechanisms that cause melt generation and ascent. The Cenozoic saw the development of numerous volcanic provinces on the African plate, including within the Central Hoggar, located in Northwest Africa, part of the Tuareg shield. The magmatic activity began at approximately 34 Ma and continued throughout the Quaternary. In order to understand the origins and potential mechanisms that generated the intraplate volcanic activity in the Central Hoggar we aim to image the subsurface architecture, in terms of electrical resistivity, from the surface to the lithospheric mantle. To do so we use magnetotelluric measurements from 40 locations to generate a 3-D electrical resistivity model, over an area of about 100 km by 160 km. Low-resistivity features (i.e., conductors) are observed in the crust that are narrow, linear structures congruent with the boundaries of terranes and prominent fault zones (e.g., Azrou N'Fad). They likely reflect the Pan-African mega-shear zones, which were reactivated throughout the tectonic evolution of the region. The model reveals that these faults are lithospheric-scale. The low-resistivity features likely represent the signatures of past fluid pathways and mineralization. A deeper low-resistivity feature is observed in the upper lithospheric mantle directly beneath the Manzaz and Atakor volcanic districts. It may represent local, small-scale metasomatism of the sub-continental lithospheric mantle, and low-percent partial melting, that sits above a regional, large-scale asthenospheric upwelling associated with the Hoggar swell. It is likely the origin point of the fluids responsible for the overlying anomalies. The results highlight the control of the lithospheric-scale, mega-shear zones on the spatial distribution of the recent Cenozoic volcanic activity, which was influenced by the location of pre-existing structural weaknesses.

1. Introduction

The surface of the Earth is made up of numerous rigid plates, and most (~95 %) volcanic activities are associated with the lithospheric boundaries of these plates (e.g., Decker and Decker, 2005). These plates move together (e.g., convergent motion), for example in subduction zones (e.g., Antilles, Indonesia, Japan, Andes, etc.), generating magmatism, or move apart (e.g. divergent motion), for example at mid-ocean ridges (e.g., Iceland) or continental rift zones (e.g., East Africa), allowing magma to reach the surface.

Another type of volcanism, which is less common and is distinct due to its location far from plate tectonic boundaries (i.e., within a plate) and its typically deep origins, is known as hotspot volcanism (e.g., Schmincke, 2004). This type is known to generate isolated islands, such as the Hawaiian archipelago or those of Polynesia. This type of volcanism is less common on continents because of the generally rather much thicker lithosphere. Most hotspots are attributed to a fixed, deep-rooted, mantle thermal plume source with the lithospheric plate moving over it, leaving a time-progressive chain of volcanoes (e.g., Hawai'i). However, some

* Corresponding author.
E-mail addresses: Z.Boukhalfa@craag.dz (Z. Boukhalfa), M.J.Comeau@tudelft.nl (M.J. Comeau).

https://doi.org/10.1016/j.gr.2024.08.003
1342-937X/

examples lack this time progression, and may also lack the strong thermal anomaly associated with a long-lived plume, thus requiring a new source model.

Therefore, continental intraplate volcanic systems are not well studied and, as a result, are not well understood. Currently, the crustal and lithospheric mantle structure of continental intraplate volcanic systems remains enigmatic and there is no consensus on the mechanisms that can cause melt generation and ascent. In contrast to well-developed modern theories for transcrustal arc magmatism (e.g., Cashman and Sparks, 2013), geochemical evidence from continental intraplate volcanism does not demonstrate crustal magma evolution or storage (e.g., Harris et al., 2010; Tschegg et al., 2011; Brenna et al., 2018), and points to mantle generation and rapid crustal ascent. Mechanisms that have been proposed to explain this activity are focused on those capable of producing mantle upwellings, including edge-driven convection, deep slab tearing or slab detachment, buoyant decompression melting, hydrous melt upwelling from stagnating piles at the mantle transition zone, and shear-driven upwelling (King and Anderson, 1998; Wortel and Spakman, 2000; Raddick et al., 2002; Conrad et al., 2011). In any case, the nature of the magma source reflects past major geodynamic events and provides information on lithosphere-asthenosphere interactions.

Cenozoic continental intraplate volcanism is well presented in the Hoggar region of southern Algeria, with evidence for numerous volcanic episodes (Liégeois et al., 2005). This region is part of the Tuareg shield, which is made of Precambrian rocks and possibly dozens of terranes, and has a high topography (1,000–3,000 m above sea level in the Hoggar) as part of a large-scale Cenozoic swell (Liégeois, 2019). Evidence suggests that the swell may have existed during the Cretaceous (Liégeois et al., 2005; Rougier et al., 2013), highlighting the importance of understanding vertical motions in the lithosphere.

The Hoggar is characterized by submeridian transcurrent mega-shear zones (Liégeois, 2019), which divide it into three parts (western, central, and eastern Hoggar). These shear zones played an essential role in the creation and evolution of the Hoggar region, which was assembled during the Pan-African orogeny by collision and accretion between juvenile terranes and ancient (Archean and/or Paleoproterozoic) terranes (Liégeois, 2019). These processes of continental growth were part of the development of central Gondwana from 870-520 Ma (e.g., Meert and Lieberman, 2008). The remobilization of these mega-shear zones during the Phanerozoic influenced the establishment of the Cenozoic volcanism in the Central Hoggar (Liégeois et al., 2005).

The origin of this activity is currently subject to debate. For example, Aït-Hamou et al. (2000) proposed that the exhumation of the Tuareg shield, possibly pre-dating but thought to be related to the recent Cenozoic intraplate volcanism (Dautria et al., 1988), was related to a mantle plume. In contrast, linear delamination occurring along suture zones (mega-shear zones) after the rotation (anti-clockwise) of the African plate and its collision with the Eurasian plate was the explanation set forth by Liégeois et al. (2005).

As a consequence of the lack of high-resolution, deeply-penetrating geophysical data, the crustal and lithospheric mantle structures of this region are not fully known and the origins and mechanisms of the continental intraplate volcanic activity remain controversial. In order to better understand the underpinning mechanisms that lead to melt generation, both here and in other intraplate systems worldwide, it is necessary to image the underlying structure of these formations. Additionally, the terranes that make up this system are of significant economic interest because they contain a wealth of mineral deposits, and for this reason too it is advantageous to map the subsurface structure and examine the potential pathways of ore-forming fluids.

Therefore, magnetotelluric (MT) surveys were carried out to investigate the Hoggar region, notably by Bouzid et al. (2008, 2015), Boukhalfa et al. (2020), and Deramchi et al. (2020). In the present study, we combine new and old measurements in an extensive dataset and apply a more accurate modelling strategy. This work was carried out to investigate the nature and origin of the Cenozoic volcanic activity in the Central Hoggar region, specifically in the Atakor and Manzaz ditricts, and to explore the influence of the mapped shear zones on its formation. In this study, we generate a 3-D electrical resistivity model of the lithosphere from the MT data. We analyse and interpret the electrical resistivity signatures and distribution in light of the available geological and geochemical data and geodynamic models, offering new insights into the structure and evolution of the intraplate system.

In addition to the regional significance, aspects of the results of this work are applicable to other continental intraplate volcanic systems worldwide, despite their distinct characteristics, including those in the Carpathian-Pannonian region in central Europe, the Eifel region in Germany, eastern Australia, central and eastern Mongolia, and northeast China.

2. Geological background

2.1. Geological and tectonic setting

At the level of the African plate, the Hoggar swell (or dome) extends over an area of approximately 500,000 km^2, with a diameter of about 1,000 km (e.g., Liégeois, 2019). It is located approximately 1,500 km south of the Mediterranean Sea. It connects to other regions including Aïr (Niger; ~700 km to the south) and a bulge extends to Tibesti (Chad; ~1,300 km to the east) and Darfur (Sudan; ~2,300 km south-east) (Fig. 1a). Further away, Cenozoic volcanism also exists in the Cameroon chain (~2,300 km south) and the East African rift (>4,000 km south-east) (see Fig. 1a).

The Atakor/Manzaz massif, part of the Hoggar volcanic province, is located in the LATEA metacraton, at the limit of the Azrou N'Fad, Égéré-Aleksod, and Tefedest terranes (LATEA is an acronym made from the names of the five main terranes; cf. Liégeois, 2019). This complex, which belongs to the Tuareg shield, sits between the West African Craton and the Sahara metacraton.

One of the most salient features of the Hoggar is its morphology, presented as a large-scale, high elevation dome or swell. In some places, the Precambrian metamorphic basement can be found at altitudes up to 2,400 m. The highest point reaches an elevation of 2,918 m (Mount Tahat), located in the volcanic district of Atakor (Lesquer et al., 1990; Rougier et al., 2013). The mechanism, and timing, of the origin of this morphology remain debated. The existence of Cretaceous sedimentary basins resting directly in discordance on the Precambrian metamorphic basement of the Hoggar, at Serouanout (Derder et al., 2023) or the In Ouzzal for example, suggests that a pulse of uplift occurred in the Hoggar in the Cretaceous (Liégeois et al., 2003). In addition, both fission track data on apatites (Rougier et al., 2013) and profile modelling of the main wadis of the Hoggar (Roberts and White, 2010) point to a pulse of uplift occurring in the Hoggar in the Eocene, directly before the beginning of Cenozoic volcanic activity, possibly as part of a long-lived structure (cf. Aloui et al., 2012).

At Hoggar, the swell is associated with intense Cenozoic magmatic activity that is grouped geographically into eight districts (Fig. 1b). Most of the volcanic massifs are distributed near the

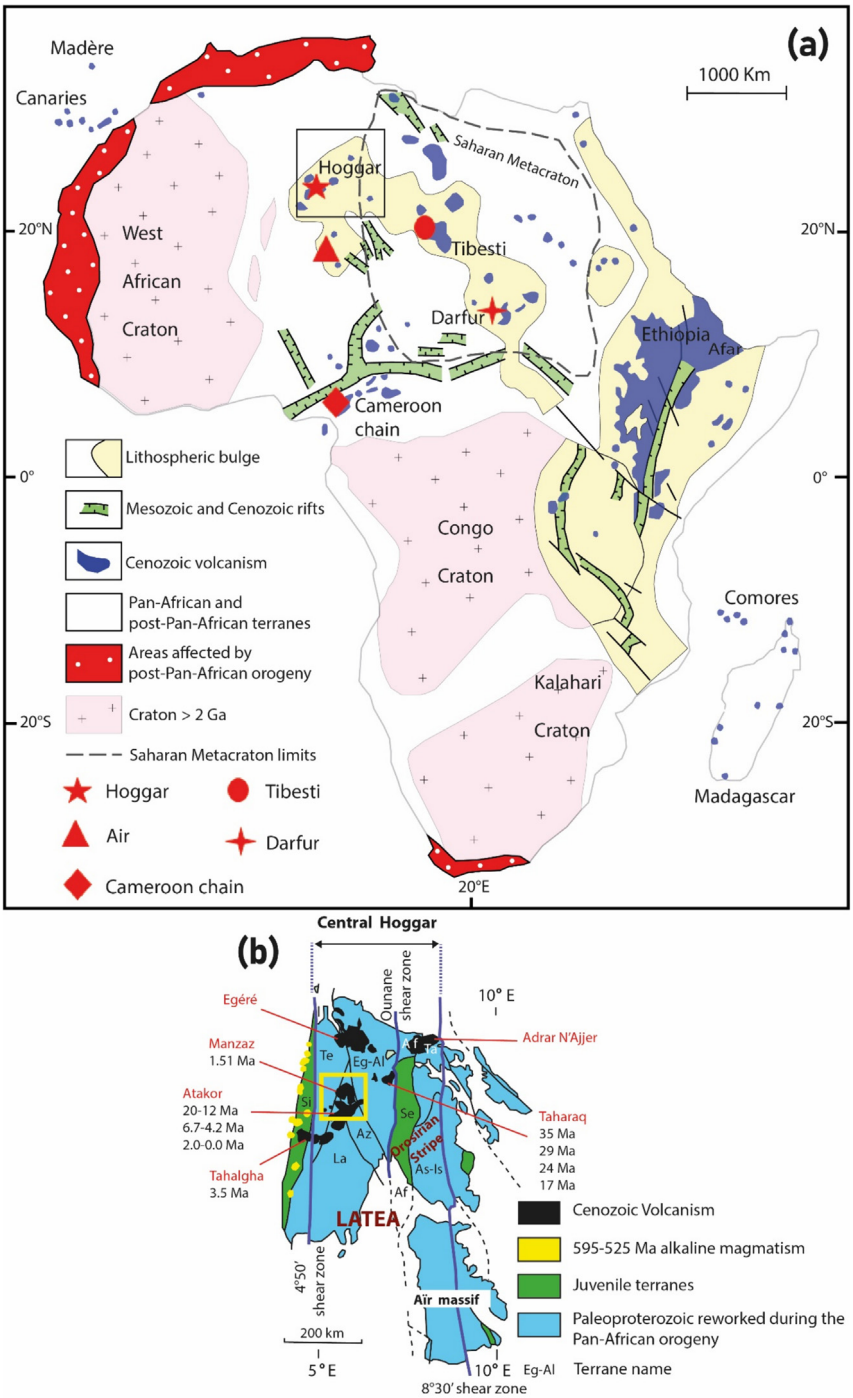

Fig. 1. (A) A simplified map of the tectonic entities of the African Plate. The LATEA region is indicated with a black box. The map highlights regions of volcanism (Hoggar: Cenozoic; Air: 28–0.7 Ma; Cameroon chain: 60–30 Ma and 30 Ma – present; Tibesti: Cenozoic; Darfur: 36–4.3 Ma). The volcanic provinces are modified from: Choubert and Faure-Muret, 1975; Black, 1984; Vail, 1985; Popoff et al., 1982; Baudin, 1986; Lasserre et al., 1977. Cratons and Metacraton: Black, 1984; Liégeois et al., 2013. Rifts are modified from: Choubert and Faure-Muret, 1975; Mougenot et al., 1986; Béa, 1987; Schandelmeier et al., 1987; Daly, 1988; Popoff, 1988; Franz et al., 1994. b) Inset of the LATEA region showing the main volcanic districts associated with the Hoggar swell/bulge, and the ages of the volcanic formations (from Aït-Hamou et al. 2000, Benmessaoud, 2014, Benhallou et al. 2016; see Liégeois et al., 2005, and Liégeois, 2019). The yellow square marks the area examined in this study. La: Laouni, Az: Azroun'Fad, Te: Tefedest, Eg-Al: Egéré-Aleksod, Se: Sérouenout, Af: Afara, Ta: Tazat and As-Is: Assodé-Issalane, Si: Silet. (For interpretation of the references to colour in this figure legend, the reader is referred to the web version of this article.)

central Hoggar dome. The total volume of solid eruptive products emitted is estimated to be 1,650 km^3, and potentially up to 2,500 km^3 if the amount lost due to erosion is taken into account (Benhallou et al., 2016). The Atakor, Manzaz, and Egéré districts appear to be controlled by a lineament trending in the N-S direction (Benhallou, 2018).

2.2. Geochemical and petrological background

The Cenozoic volcanism of the Hoggar is of intraplate alkaline type. Two groups of magmatic rocks have been identified from field and petrological observations: one mafic and one felsic (Girod, 1971; Benhallou, 2000; Yahiaoui, 2003; Azzouni-Sekkal

et al., 2007). The mafic group is related to the formation of uplifted plateaus, scoria cones, and lava flows. The felsic group includes pyroclastic formations in addition to the domes, necks, and spines observed across the landscape.

In the Atakor, (Girod, 1971; Yahiaoui, 2003; Azzouni-Sekkal et al., 2007) the mafic group is composed of basalt and basanite, mainly silica-undersaturated types, including phonotephrite. In the felsic group, two diverging trends are observed: one trend is characterized by intermediate silica (silica-undersaturated) and increasing alkali contents, from trachyte-phonolite; the other trend, has increasing silica contents (silica-saturated), from benmoreite-trachyte-rhyolite.

South of Atakor, the Taessa lavas (Megueni and Boussisse, 2017; Benhallou et al., 2019) (mainly basanite, alkali basalts) show homogeneous compositions for major elements ($41.49 \leq SiO_2 \leq 47.78$ wt%; $3.40 \leq (Na_2O+K_2O) \leq 4.52$ wt%) and trace elements ($602 \leq Sr \leq 1027$ ppm; $196 \leq Zr \leq 279$ ppm; $50 \leq Cr \leq 434$ ppm; $72 \leq Ni \leq 271$ ppm). The Taessa lavas have a geochemical composition largely similar to those of the typical Hoggar lavas but seem to be less evolved and more primitive.

North of the Atakor, the Manzaz volcanic zone has distinct characteristics (Benhallou et al., 2016; Benhallou, 2018), and contains very homogeneous erupted lavas. Benhallou et al. (2016) reported that the loss on ignition (LOI) is less than 1.5 %; this can indicate that the samples are fresh, but it is not zero, which suggests the presence of minerals containing the hydroxyl ion (OH). The chemical compositions, recalculated with a total of 100 % on an anhydrous basis (i.e., H_2O and CO_2 free), were used to classify the rocks in a TAS diagram (see Fig. 2). Basic rocks ($45 < SiO_2 < 52$ %) are abundant, including basanites found in all volcanic units, and their silica-poor compositions are primitive, suggesting that they may have originated directly from the upper mantle (Benhallou et al., 2016, and references therein). In addition to the dominant basanite, alkali basalt and trachybasalt are identified, as well as trachyandesite in an older lava flow. The Manzaz suite is characterized by the occurrence of olivine (with fosterite contents of Fo88-Fo56). Mantle olivine (magnesium-rich, with fosterite fractions of Fo88-Fo87) is identified in some basanites and alkali basalts (Benhallou et al., 2016). Plagioclase has anorthite fractions ranging from An61 to An30 (Benhallou et al., 2016). Lucas et al. (2016) remarked that tephra, ash, and tuffs deposited around the numerous intact scoria cones of the Manzaz massif contain megacrysts (up to 1 cm in size) of titanium-rich amphibole (magnesio-hastingsite), magnesium-rich olivine (Fo94), clinopyroxene (diopside), titanite, and sodium-rich plagioclase (oligoclase). Benhallou et al. (2016) noted the occurrence of amphibole microcrysts in the Manzaz suite, including in the most primitive rocks (for example edenite in the basanites). In many samples, extensive evidence for hydrothermal alteration exists (Benhallou et al., 2016).

Thermobarometry studies on amphibole megacrysts conducted by Lucas et al. (2014) and Benhallou (2018) indicated a magma reservoir at the crust-mantle boundary (depth of 32–34 km) where amphiboles crystallized for some volcanic edifices. There were also indications for other intermediate depths where pyroxenes may have crystallized, for example at a depth of 25 km. According to Azzouni-Sekkal et al. (2007), the presence of mantle-derived amphibole megacrysts and peridotite mantle xenoliths (Beccaluva et al., 2007) in addition to the nonprimary chemical compositions of the magmatic rocks in the Atakor and Manzaz volcanic districts suggest that magmatic differentiation likely occurred in the upper mantle.

Isotopic and trace element data from xenoliths (Beccaluva et al., 2007) suggest that the lithospheric mantle beneath the Manzaz district was rejuvenated, and that lithospheric removal and replacement by an upwelling asthenosphere may have occurred. Similarly, other authors consider that the primary magmas were produced as a consequence of low degrees of partial melting due to decompression at variable depths (e.g., 40 to 110 km) in an upwelling asthenosphere (Liégeois et al., 2005; Azzouni-Sekkal et al., 2007; Benhallou, 2018). Whether such upwelling was induced by a lithospheric step, due to the thick lithosphere below the cratonic area to the west compared to the LATEA, or by some other delamination-style event is not known. Complementary to this, recent models, based on the subsurface electrical resistivity distribution, demonstrate the role of linear, lithospheric-scale, mega-shear zones on the spatial distribution of volcanism and the influence of fluids and mineralization associated with Cretaceous-Cenozoic events on the current structure of the Hoggar (Bouzid et al., 2015; Boukhalfa et al., 2020; Deramchi et al., 2020). A mantle plume or hot-spot model, although originally deemed

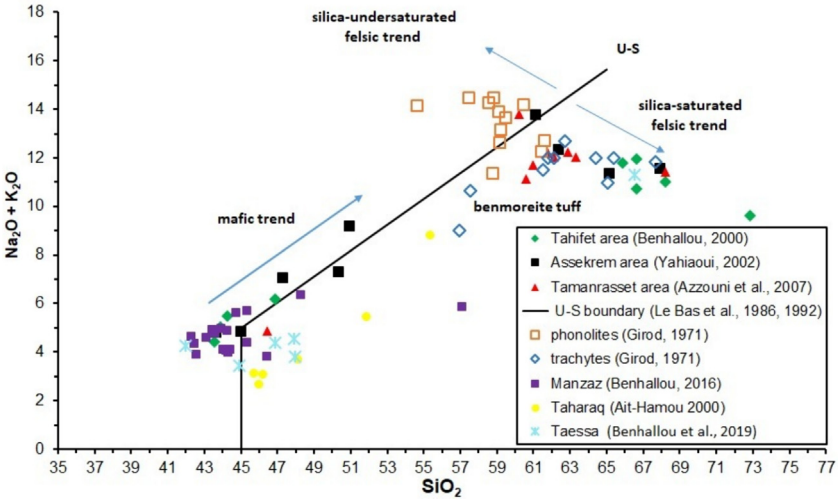

Fig. 2. A compilation of Hoggar volcanic rock compositions shown in a total alkali-silica (TAS) diagram. The values are recalculated on a H_2O– and CO_2-free basis (Le Bas et al., 1986, 1992; Le Maitre et al., 1989; Le Maitre, 2002). The silica undersaturated-saturated boundary (US) is indicated (black line). The diagram is modified from Azzouni-Sekkal et al. (2007) and Benhallou et al. (2016). The compilation references the following studies: 1, filled diamond, Tahifet area (Benhallou, 2000); 2, filled square, Assekrem area (Yahiaoui, 2002); 3, filled triangle, Tamanrasset area (Azzouni et al., 2007; 4, open square, phonolites (Girod, 1971); 5, open diamond, trachytes (Girod, 1971); 6, small filled square, Manzaz (Benhallou, 2016); 7, circle, Taharaq (Aït-Hamou, 2000); 8, cross, Taessa (Benhallou et al., 2019).

attractive (Aït-Hamou and Dautria, 1994, 1997; Aït-Hamou, 2000; Aït-Hamou et al., 2000; Courtillot et al., 2003), is inconsistent with much geophysical evidence (Lesquer et al., 1989; Ayadi et al., 2000; Bouzid et al., 2015; Boukhalfa et al., 2020; Deramchi et al., 2020). Despite the various explanations and hypotheses set forth, no model has yet prevailed, and the debate on the origins of the Hoggar and the Tuareg shield is ongoing.

2.3. Previous geophysical studies

Knowledge of the lithospheric structure beneath the Hoggar region remains imperfect due to low spatial resolution and gaps in the distribution of the existing geophysical data. This limited knowledge of the crust and mantle structure has led to contradictory interpretations and conflicting ideas. In the 1960s and 1970s, surveys of scalar aeromagnetic data attempted to covered the entire Algerian territory (Bournas et al., 2003; Boubekri et al., 2015; Harrouchi et al., 2016, 2020). The coverage of high-resolution ground-based gravity measurements is low, especially in the Central Hoggar region and particularly in the Atakor and Manzaz districts (Lesquer et al., 1989; Brahimi et al., 2018), however, modern space-based measurements (e.g., GRACE) have led to good regional-scale coverage.

A strong negative Bouger gravity anomaly (−100 to −140 mgal) has been revealed beneath the Hoggar swell, with a diameter of more than 400 km, and is centered on the Atakor volcanic district (Liu and Gao, 2010; Lesquer et al., 1989). There has long been controversy regarding the density structure beneath the Hoggar swell. Some models (Brown and Girdler, 1980) attribute the gravity anomaly to a thinned lithosphere (60 km thick) from an initial thick state (100 km thick), or similarly, to the presence under the base of the crust of a light body with a lateral extent of hundreds of kilometers (Lesquer et al., 1988). In contrast, Liégeois et al. (2005) hypothesized a much deeper source of the anomaly, at depths greater than 200 km (i.e., in the asthenosphere).

A strong heat flow anomaly (up to 120 mW/m^2) is observed in the adjacent Saharan sedimentary basins (Takherist and Lesquer, 1989; Lesquer et al., 1990). However, an average value of 53 mW/m^2 (from 13 measurements) is observed in the Hoggar region. This value is comparable to those determined for Precambrian massifs (Lesquer et al., 1989). The northern part of the Hoggar (north of Tamanrasset city) contains no heat flow data.

In Northwest Africa, tomographic models computed at the African or global scale highlight the main tectonic units such as cratons or mobile belts (Sebai et al., 2006; Fishwick and Bastow, 2011; Ouattara et al., 2019). These models are unable to resolve features of a small size (<100 km; e.g., narrow terranes or local volcanic districts), because of their limited lateral resolution. The tomographic models show fast and thick cratonic zones (West African Craton) juxtaposed with slower and thinner Pan-African mobile belts. No significant seismic signature was described in the upper mantle beneath Hoggar. Ayadi et al. (2000) carried out a local-scale P-wave tomography experiment, along a linear profile roughly connecting In Salah in the north to Tamanrasset in the south, that provided seismic velocity models with a better resolution and highlighted a low-velocity zone and low density under the Atakor and Tahalgha (~100 km south) volcanic districts (central Hoggar) in the upper mantle that extends down to approximately 300 km depth.

Liégeois et al. (2005) suggested significant topography of the base of the lithosphere with the depth to the base varying from about 200 km beneath the Archean terrane (In-Ouzzal Granulitic Unit) to about 100 km beneath the juvenile Pan-African terranes, based on both geological arguments and seismic tomography data. In this scenario, the lithosphere under the LATEA metacraton would have an intermediate thickness of about 160 km.

However, recent results contradict this supposition. According to Lemnifi et al. (2020), who undertook a seismic S-to-P receiver function study beneath much of northern central Africa, the thickness of the lithosphere under LATEA varies from approximately 70–85 km around the village of Tamanrasset and becomes thinner towards the east until it reaches about 60–70 km under the eastern edge of LATEA, with the smallest thickness detected below the Hoggar volcanic province. These values are in agreement with the study by Gangopadhyay et al. (2007), which showed a strong decrease in P-wave velocity at a depth of 80 km under the GEOSCOPE station of Tamanrasset. The crustal thickness estimated by Liu and Gao (2010), based on seismic receiver functions, is about 34 km below the TAM station (near the village of Tamanrasset). This agrees with the previous estimate given by Gangopadhyay et al. (2007) of approximately 36 km under the same station.

For its part, electromagntetic data, and in particular MT data, have been collected across parts of the Hoggar in several surveys. However, considering the large extent of the region, the data coverage is not uniform and is incomplete. The surveys consist of a combination of large reconnaissance profiles (e.g., with a measurement spacing of 40 km or more) and small local profiles (measurement spacing of 5 to 15 km), but no continuous model yet exists for the separate surveys. Previous models derived from MT data in the Hoggar (Bouzid et al., 2015; Boukhalfa et al., 2020; Deramchi et al., 2020) revealed a resistive upper crust overlying a conductive lower crust and a moderately to highly conductive lithospheric mantle. Models of the western Hoggar affirmed the boundaries of Archean In-Ouzzal granulitic units and the adjacent Pan-African basement (Bouzid et al., 2008).

3. Magnetotelluric data acquisition and analysis

3.1. The magnetotelluric method

The MT method is a geophysical technique that uses the time variation of electric and magnetic fields at measurement stations located on the surface of the Earth to probe the subsurface electrical resistivity structure. Natural electromagnetic signals are generated in the atmosphere and ionosphere/magnetosphere over a broad range of frequencies, and the penetration depth of the electromagnetic signals (the skin depth) depends on the bulk resistivity of the subsurface and the signal frequency (e.g., Unsworth and Rondenay, 2012). The frequency-dependent, complex-valued, impedance tensor is converted to an apparent resistivity and an impedance phase (e.g., Unsworth and Rondenay, 2012). The impedance tensor, $\boldsymbol{Z}$, links the horizontal electric (E) and magnetic (H) fields,

$$E(\omega) = Z(\omega)H(\omega) \tag{1}$$

where ω is the angular frequency, and is written as

$$\boldsymbol{Z} = \begin{pmatrix} Z_{xx} & Z_{xy} \\ Z_{yx} & Z_{yy} \end{pmatrix} \tag{2}$$

The apparent resistivity (ρ_a) and impedance phase (ϕ) are written as

$$\phi_{ij} = \tan^{-1}\left(Z_{ij}\right) \tag{3}$$

and

$$\rho_a = \frac{|Z_{ij}|^2}{\omega\mu_0}, \tag{4}$$

where *ij* represents the component of the impedance tensor, σ is the conductivity (inverse of resistivity, ρ), μ_0 is the magnetic permeability of vacuum, and ω is the angular frequency.

The technique is particularly sensitive to the presence of interconnected low-resistivity material and has been used extensively to image local and regional fault and suture zones (e.g., Türkoğlu et al., 2008; Comeau et al., 2020a; Sheng et al., 2021), explore large-scale tectonics and lithosphere-asthenosphere interactions (e.g., Wannamaker et al., 2008; Ostos and Park, 2012; Käufl et al., 2020; Wang et al., 2022; Jin et al., 2022), investigate deep imprints of mineral systems (e.g., Heinson et al., 2006; Comeau et al., 2022a; Sheng et al, 2022), and characterize volcanic and magmatic pathways and sources (e.g., Bertrand et al., 2012; Samrock et al., 2021; Comeau et al., 2022b; Unsworth et al., 2023).

3.2. Data collection and processing

The MT data used in the present study come from 40 broadband measurement sites that form a 3-D distribution roughly oriented NE-SW (Fig. 3). Some measurements, 18 sites forming a NE-SW profile (i.e., the southern profile), were analysed by Bouzid et al. (2015) and used to generate a two-dimensional (2-D) model, which did not consider the full impedance tensor and made assumptions about the underlying structure. The other measurements, 22 sites, are being analysed and modelled for the first time.

A total of 15 MT measurement sites (names: mnz01 to mnz15) were arranged in two cross profiles (roughly oriented NE-SW and NW-SE), covering the Manzaz district. They were collected during the period from December 2016 to January 2017. The equipment used was the Phoenix Geophysics of Canada V5 System 2000 consisting of non-polarizable electrodes on two perpendicular dipoles ~100 m long and three induction coil magnetic sensors oriented mutually orthogonal. These data complemented an existing 13 sites (names: atk01 to atk13), collected with the same equipment in April 2012 along a parallel NE-SW profile, which focused on the northern part of the Atakor district and is centered on the village of Idelès (see Bouzid et al., 2015). The rest of the measurements were collected during previous broad reconnaissance surveys of the Hoggar massif: 5 sites (hog26, hog27, hog30, hog31, and hog32) were collected in January/February 2005, 3 sites (hog10, hog11, and hog12) in April 2003, and 4 sites (hog02, hog03, hog06, and hog07) were collected in 1993 (with an older V5 system). The spacing between measurement sites varies from 5 km to 10 km, except for some sites (hog03, hog26, hog32, and hog30) that are scattered around the area to provide 3-D coverage (spacing of ~20–40 km).

\The recordings were carried out for approximately one day. This is sufficient to record deeply-penetrating signals, reaching depths beyond the base of the crust, because the Hoggar region is a favourable setting mostly devoid of electrically conductive sedimentary basins. Furthermore, the region is far from heavily populated areas that create anthropogenic electromagnetic noise and, as a result, the data were of good quality and typically did not need a permanent remote reference station to reduce noise.

The time series data were processed using the code of Phoenix Geophysics, which is based on a statistically-robust technique. The frequency-dependent impedance tensor is used to estimate the apparent resistivity and impedance phase and the tipper is derived from the transfer function of the vertical to horizontal magnetic fields (related to the induction vector) (Fig. 4). The data are generally very smooth and have low error bars. At some sites, the long periods (low frequencies) up to more than 3,000 s show some scatter with larger error bars (e.g., site atk10 in Fig. 4).

3.3. Data analysis and dimensionality

Overall, the apparent resistivity curves have similar shapes. For short periods (<0.1 s) they show a moderate resistivity of ~1,000 Ωm and increase up to 10,000 Ωm (maximum at approximately 0.1–1 s), and at longer periods (100–1,000 s) the resistivity decreases to 10–100 Ωm. This bell shape is considered to be somewhat typical for the lithosphere of cratonic zones, with a high-resistivity upper crust and a low-resistivity mantle. However, the transition here appears to occur at a period of about ~1 s, approximately in the mid-crust at ~16 km depth based on simple skin-depth calculations, implying a low-resistivity lower crust.

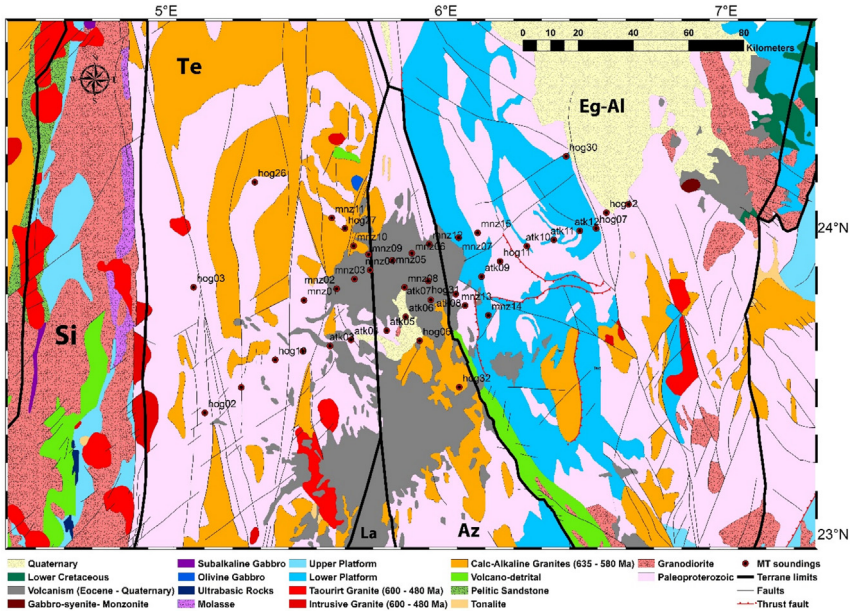

Fig. 3. Distribution of magnetotelluric (MT) measurements (red circles) on a geological map of the Atakor and Manzaz districts (Bertrand and Caby, 1977; Liégeois, 2019, and references therein). Site names are given. The main terranes comprise a metacraton and are labelled. La: Laouni terrane; Az: Azrou'N'Fad tarrane; Te: Tefedest terrane; Eg-Al: Egéré-Aleksod terrane; Si: Silet terrane. (For interpretation of the references to colour in this figure legend, the reader is referred to the web version of this article.)

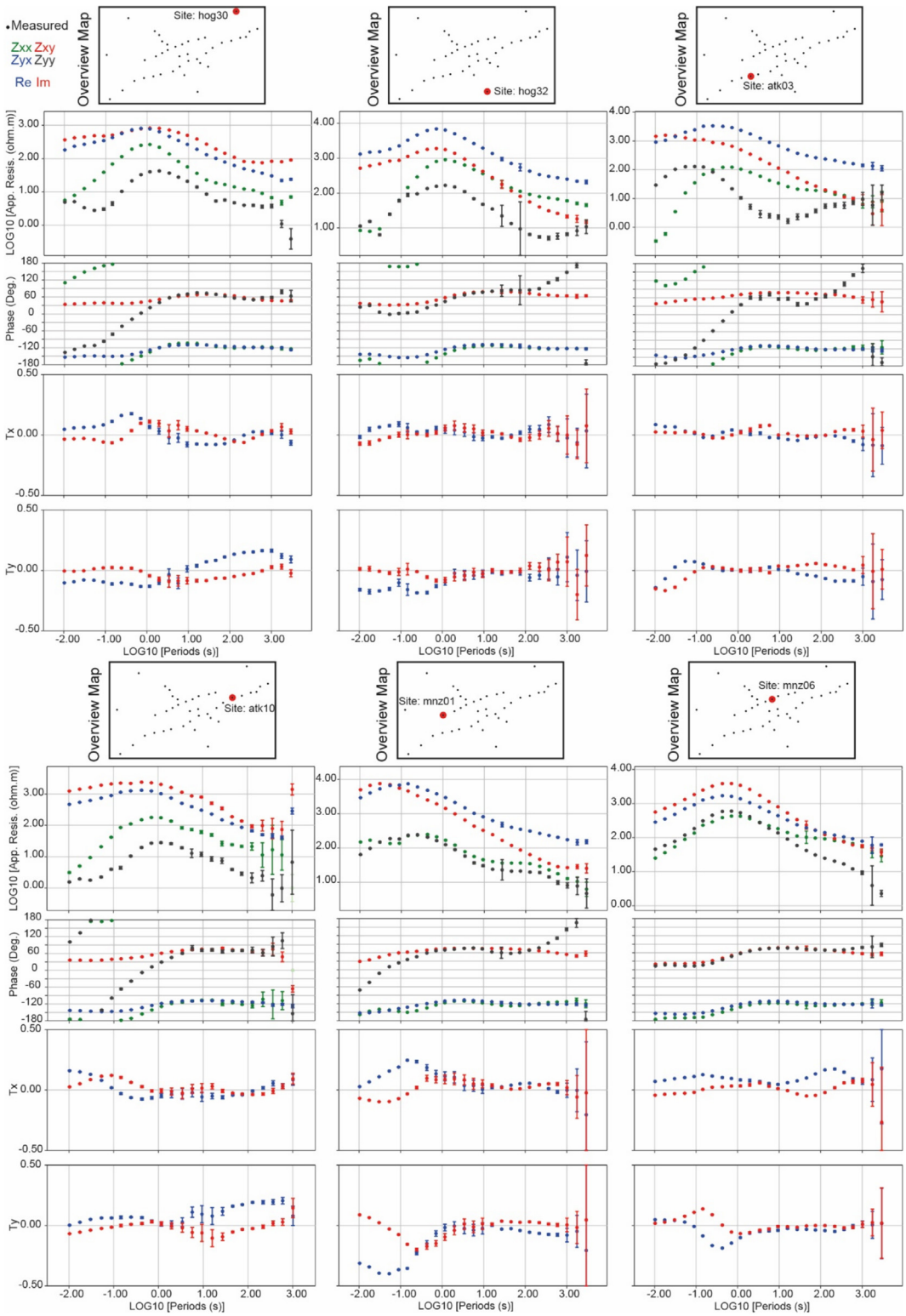

Fig. 4. Apparent resistivity (ρ_a), impedance phase (Φ), and tipper (T) components for six representative magnetotelluric measurements, plotted against period (s).

The curves for the off-diagonal impedance elements of the sites in the central and western parts of the area are characterized by separation at long periods, and the YX component above the XY component (e.g., sites hog32, atk03, and mnz01 in Fig. 4). In contrast, the curves for the off-diagonal elements of the sites located to the east are characterized by similarly shaped curves with no long period separation, and the XY component above the YX component (e.g., sites atk10, mnz06, and hog30 in Fig. 4). The tipper components range between 0.1 and 0.5, with most variations observed at the high frequencies (below 1 s).

Prior to modelling, careful analysis of the impedance tensor and tipper data should be performed to determine the appropriate dimensionality of the subsurface structure. For this purpose, the phase tensor method (Caldwell et al., 2004; Bibby et al., 2005;

Booker, 2014) is particularly suitable, because it is not affected by galvanic distortion effects. It is commonly represented by an ellipse. This ellipse reduces to a circle in the case of one-dimensional earth. For a 2-D subsurface, the axes of the ellipse determine the geo-electric structural direction or strike. Caldwell et al. (2004) defined a dimensionality indicator called skew (symbol β) calculated from the components of the phase tensor. If the value is less than a threshold, typically taken to be 3°, the MT data can be described by a 2-D model. In this case, the real parts of the induction vectors should be consistent with the direction given by the ellipse of the phase tensor, i.e., perpendicular to the strike. If the skew value exceeds the threshold, then it is indicative of 3-D structures. In that case, it becomes necessary to use a 3-D model to properly represent the data.

Phase tensor ellipses were plotted for different periods (Fig. 5) corresponding to different depths, from the upper crust and mid-crust to the lower crust and lithospheric mantle. For the same periods, the induction vectors were plotted (pointing to conductors; Parkinson, 1962). Although the majority of the phase tensor ellipses and skew values indicate a regional 2-D subsurface, there are some measurement locations and frequencies where 3-D structure is indicated. Therefore, a 3-D model would best fit all the data and provide a more reliable model of the subsurface in this region.

Moreover, the real component of the induction vectors point toward conductive structures. At very short periods, these directions are scattered, due to local near-surface conductors; whereas at long periods they tend to agree with each other because they point to the same (large) features. The induction vectors converge at several locations, outlining zones that have a strong conductivity. Significantly, the shear zones in the central part of the study area (see Figs. 3 and 5) associated with the east and west borders of the Azrou N'Fad terrane, are aligned with these features. That is, the induction vectors detect the shear zones as conductive features and, given the periods where this is observed, they reflect the significant depth of these features, implying that they can reach the base of the crust, or possibly beyond.

4. Data modelling

4.1. Generating a 3-D model

A model of the electrical resistivity structure was generated by applying a 3-D inversion to the MT data using the finite difference code MODEM (Egbert and Kelbert, 2012), which employs a non-linear conjugate gradient (NLCG) algorithm in a parallelized version (Meqbel, 2009). The preferred 3-D resistivity model is the result of the joint inversion of the full impendence tensor (Z; four components) and the vertical magnetic transfer function (T; two components) from 40 MT measurement sites, and includes 23 periods ranging from 0.001 s to 1,000 s.

Multiple inversion runs were carried out with different parameters tested and the convergence of the inversion algorithm and the normalized root mean square (nRMS) misfit were examined. This included varying: the model grid (e.g., coarse or fine), the starting model (e.g., halfspace of 30, 100, 300, or 1,000 Ωm), the data components inverted, the smoothing parameter (e.g., covariance of 0.2, 0.3, 0.4, 0.5, and 0.6; equal in horizontal and vertical directions or different), and various data error floor settings. Some of these tests are discussed in the supplementary material document.

The preferred model grid was discretized with rectilinear cells as follows. Horizontally, cell sizes were set to 1.6 km by 1.6 km

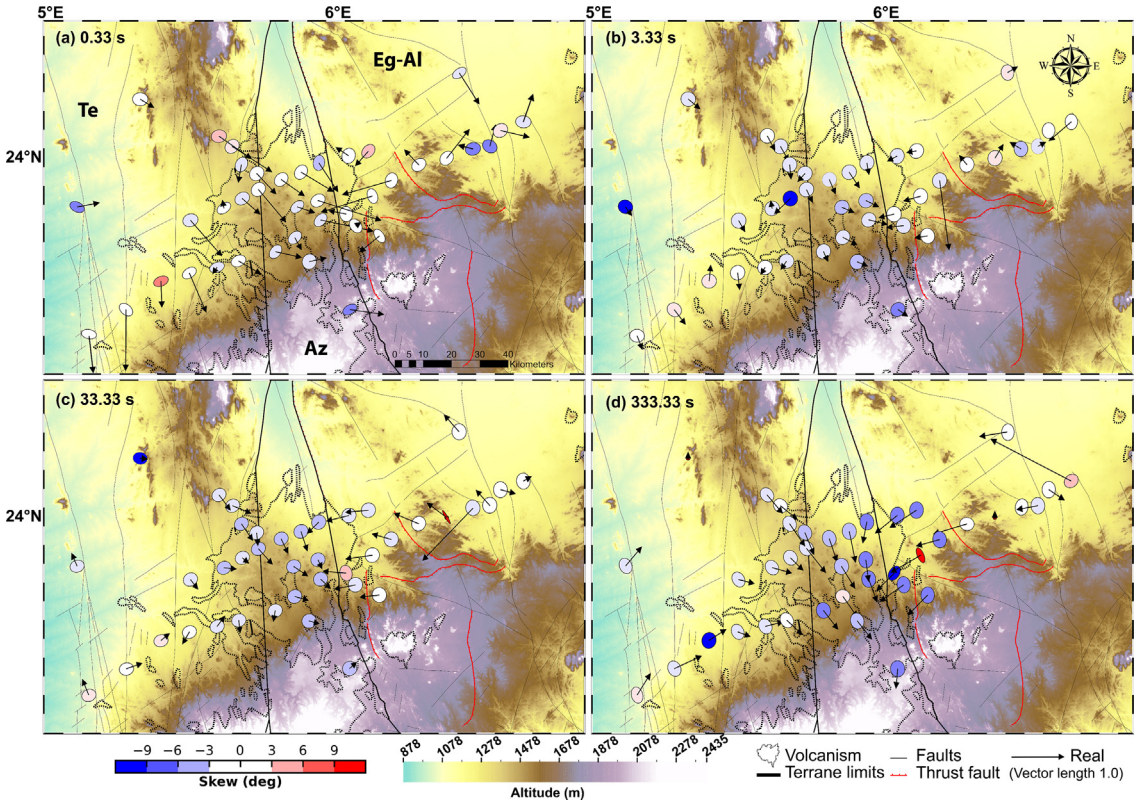

Fig. 5. Phase tensor data at each measurement site, and the real component of the induction vector (pointing to conductors, following Parkinson, 1962). These are shown for periods of (a) 0.3 s, (b) 3.3 s, (c) 33 s, and (d) 333 s. The phase tensor ellipses are coloured according to their skew value (β). Values of | β | > 3° can be interpreted as indicating 3-D structure. The length scale for the induction vectors is shown in panel a. Phase tensors were calculated and plotted with software MTpy (Krieger and Peacock 2014; Kirkby et al., 2019). The background is a topographic map. The map labels correspond to terrane names. Te: Tefedest; Eg-Al: Egéré-Aleksod terrane; Az: Azrou'N'Fad terrane.

for the inner grid, with 17 padding cells in each direction outside the site array where the sizes increased by a factor of 1.2. The cell size represents a distance of 1/3 to 1/6 of the average measurement site spacing and a few times smaller than the minimum site spacing, thereby ensuring that there are sufficient cells between measurements (see Robertson et al., 2020). Vertically, the cells started from 5 m in thickness for the topmost layer and increased by a factor of 1.15. The final model grid included 104 x 164 x 71 cells in the X, Y, and Z directions, corresponding to 519 km by 615 km horizontally and 680 km vertically. After numerous tests, the smoothing parameter was set to 0.3 for all directions, and the initial model was set to a 100 Ωm homogeneous half-space (see the Supplementary Material document).

For the impedance components, we assigned error floors of 5 % abs(Zxy) for Zxy, 5 % abs(Zyx) for Zyx, 10 % abs(Zxy) for Zxx, and 10 % abs(Zyx) for Zyy. We assigned a constant error floor value of 0.03 for the tipper components (Tx and Ty). The final model underwent 95 iterations and converged with an nRMS of 1.06. The nRMS of the starting model was 8.20. As a comparison, the nRMS was 1.01 for a model using only the full impedances and was 1.16 for a model using only tippers. Fig. 6 illustrates the model fit to the data for all components at representative sites. A site-by-site examination of the data and model response misfits (Fig. 7) shows that the model fits the data well everywhere and there is no bias to some part of the dataset.

4.2. Electrical resistivity structure

The 3-D electrical resistivity model crosses three different terrane domains (Te: Tefedest; Az: Azroun N'Fad; Eg-Al: Egéré-Aleksod terranes) and exhibits very complex electrical structure. Fig. 7 shows horizontal depth slices extracted from the model; Fig. 8 shows vertical sections extracted from the model.

The upper crust is mainly dominated by high-resistivity (1,000–10,000 Ωm; e.g., label R0). In contrast, the middle-lower crust is characterized by zones of low resistivity (from less than 1 Ωm to 10 Ωm), generally embedded in a moderately resistive background (100–1,000 Ωm). The mid-crust, depths of 10–17 km (Fig. 7b-d), shows more complex features than those at shallower depths. The distribution of resistivity is consistent with the surface geology. The most prominent feature identified is a major low-resistivity zone of less than 1 Ωm underneath the Manzaz and Atakor volcanic districts. These zones are subvertical and are elongated in the N-S direction. This is consistent with the major shear zones and terrane limits in this region, and with the orientations of some major faults. We identify and label six conductive anomalies from west to east at this level (C1, C2, C3, C4, C5, and C6). Throughout most of the crust, they are separated by the moderately resistive background (100–1,000 Ωm; features labelled R2 to R4). Starting from depths greater than 29 km, near the base of the crust (approximately 34 km) and in the mantle, conductive anomalies are interconnected, producing an extended horizontal body in the E-W and NE-SW direction.

At greater depths (>44 km), the uppermost lithospheric mantle shows an expected decrease in resistivity but also shows variable resistivity values. Specifically, values of more than 100 Ωm to the west (beneath the hog02 and atk01 MT stations; label R1), where there is no lower-crustal conductor and 10–100 Ωm in the eastern part (from atk08 to atk13; label R5). A deep sub-circular conductive body (label Cs; ∼10 Ωm) is observed in the central part of the model, directly beneath the Manzaz and Atakor volcanic districts (e.g., atk04 to atk06). A similar result was noted by Bouzid et al. (2015), based on 2-D modelling, which did not consider the full impedance tensor and imposed a geo-electric strike direction of N15W. It is significant that the conductive features at depth are spatially associated with the surface expressions of volcanism, as well as with the major shear zones and terrane limits in this region.

5. Discussion

5.1. Interpretation of upper-crustal electrical resistivity features

The subsurface electrical resistivity largely depends on the amount and type of conductive material present in the rock matrix, in addition to the temperature and pressure conditions. Conductive material can include partial melting, and/or saline aqueous fluids, and/or mineral alteration (e.g., from metasomatic processes or hydrothermal alteration; including sulfide minerals or graphite). Interpretations are facilitated by the available geoscientific evidence, e.g., from geochemical and geological studies.

The 3-D electrical resistivity model (Figs. 7 and 8) obtained in this study, reveals a high-resistivity upper crust (∼10,000 Ωm; 0–10 km depths). It is consistent with the typical properties of Precambrian upper crust (Jones, 1992). We interpret that this is likely due to the Paleoproterozoic basement and granitic rocks. Precambrian basement rocks are known in the Azrou N'Fad terrane and the adjacent Tefedest and Egéré-Aleksod terranes (Black et al., 1994; Benhallou et al., 2016 and references therein). Granitics complexes of alkaline affinity (Aïdrous-Belhocine, 2010; Benhallou et al., 2016 and references therein), which are part of the Taourirts groups of Tamanrasset (Azzouni-Sekkal et al., 2003) that were likely established in the Upper Ediacaran to Lower Cambrian (Cheilletz et al., 1992; Paquette et al., 1998), cut across all the Precambrian rock units (Boissonnas, 1973; Aïdrous-Belhocine, 2010). Some scattered conductive anomalies at shallow depths (<1 km) are likely caused by minor sediment sequences. These electrical characteristics have been observed in other districts of the Hoggar (Bouzid et al., 2015; Boukhalfa et al., 2020; Deramchi et al., 2020).

5.2. Interpretation of middle-lower crustal electrical resistivity features

Within this resistive upper crust (0–10 km depths), several lower resistivity structures exist (∼1,000 Ωm; see Fig. 8). These are linked to conductive structures (<10 Ωm) in the middle-lower crust (10–30 km depths). The transition from the upper crust to the middle crust represents a sharp step and steep reduction in the background resistivity. This has been previously observed in other regions of the Earth (e.g., Käufl et al., 2020; Comeau et al., 2020b) and is likely linked to the brittle-ductile transition zone. These features (labelled C1, C2, C3, C4, C5, and C6; Figs. 7 and 8) are oriented subvertically and are elongated in the N-S direction.

Their locations are consistent with the major shear zones and terrane limits identified in this region (e.g., F1 to F5 in Fig. 8). Furthermore, they are spatially associated with the surface expressions of volcanism. We hypothesize that the structurally weak fault/suture zones are natural pathways through the crust for volcanic fluids, and thus these features represent the architecture of the Manzaz magmatic plumbing system. Therefore, the effects of Cenozoic volcanism can be used to image the structure of a much older tectonic deformation (Neoproterozoic).

It is noteworthy that the highest conductivity values are found along submeridian faults (representing the two limits of the Azrou N'Fad terrane), and particularly where the Manzaz lavas have spread. Figs. 7 and 8 show that the conductive anomalies of the lower and middle crust are linear. They reflect the Pan-African mega-shear zones that were reactivated at different times from the post-collisional Pan-African period, with mostly transpressive

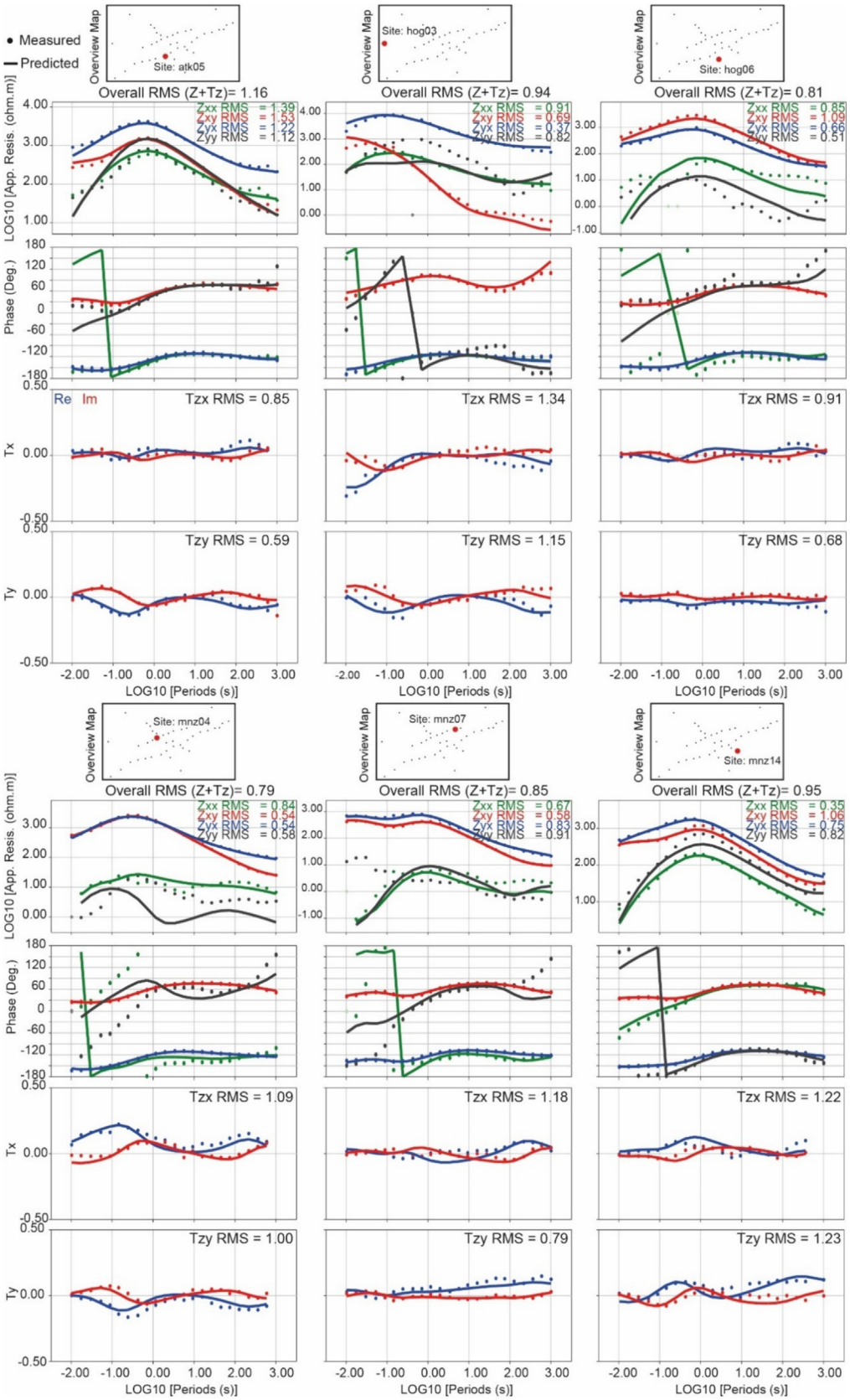

Fig. 6. Apparent resistivity (ρ_a), impedance phase (Φ), and tipper (T) components for six representative magnetotelluric measurements, plotted against period (s). The dots are the measured data and the lines are the model responses (predicted) from the 3-D model. The results demonstrate a good fit to the measured data for all components.

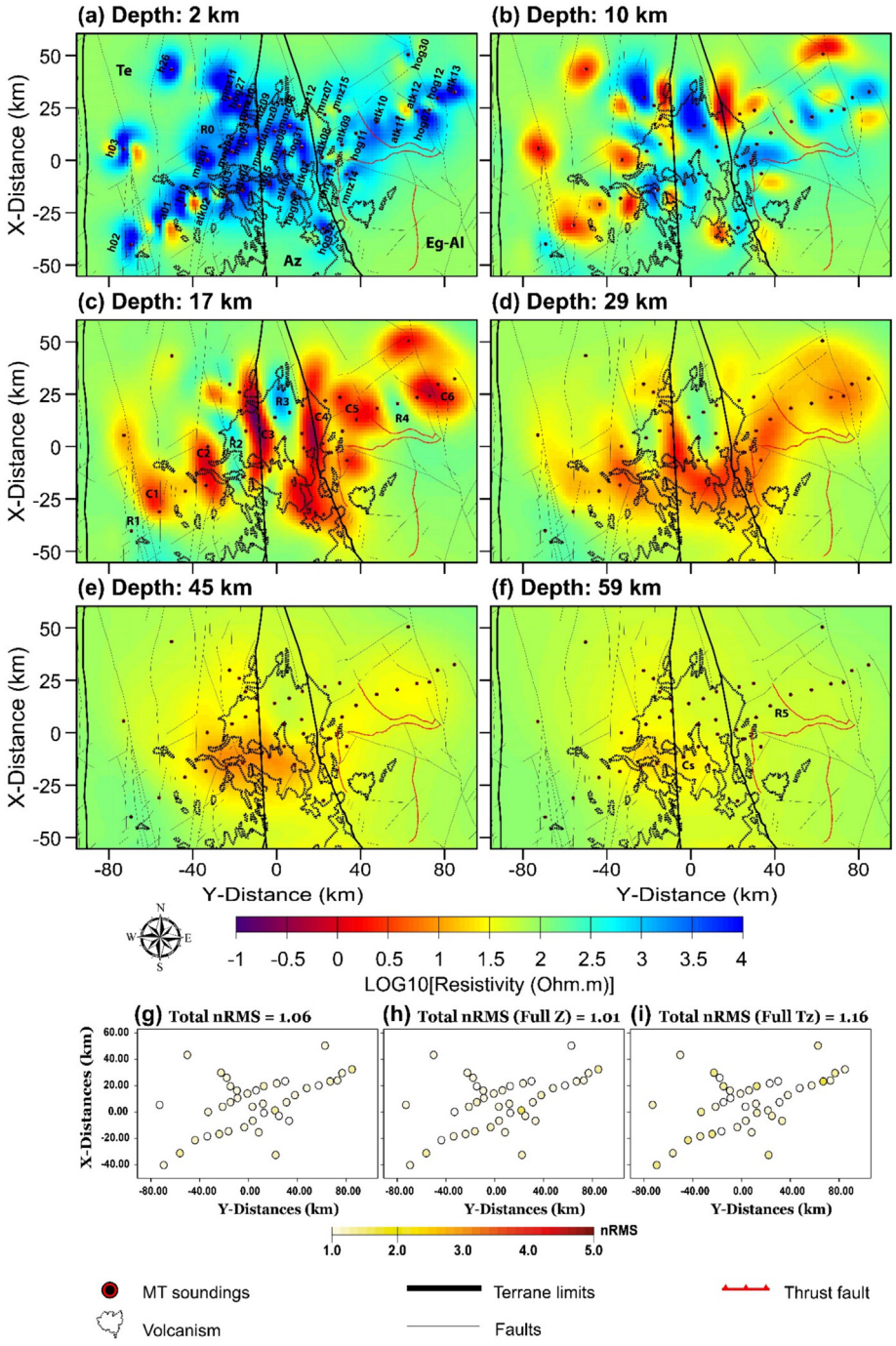

Fig. 7. (a-f) Horizontal depth slices extracted from the 3-D electrical resistivity model. Labels C1 to C6 and Cs indicate low-resistivity (conductive) anomalies; labels R1 to R4 indicate moderate-high resistivity anomalies. Site names and terrane abbreviations are displayed in panel (a). Te: Tefedest; Eg-Al: Egéré-Aleksod terrane; Az: Azrou'N'Fad terrane. (g-i) Site-by-site distribution of the normalized root mean square (nRMS) for the total model with full impedance and tipper (left), the full impedance only (centre), and tipper only (right).

movements, through to the Phanerozoic (Boukhalfa et al., 2020; Deramchi et al., 2020; Deramchi et al., 2023).

There is evidence that, regionally, the erupted lavas have homogenous compositions of major elements, trace elements, and radiogenic isotopes, indicating that these lavas have been very weakly contaminated by the basement crust, aided by re-working of the pre-existing fault zones that allow rapid ascent of magma batches (e.g., Benhallou, 2000; Liégeois et al., 2005; Ben El Khaznadji et al., 2017). Rapid ascent of magma from the mantle to the surface, has been determined for other intraplate volcanic systems (e.g., Harris et al., 2010; Tschegg et al., 2011; Brenna et al., 2018; Comeau et al., 2022b). Furthermore, there is a lack of evidence for high heat flow in this region (Lesquer et al., 1989). Therefore, long-lived crustal melt storage is not expected.

The subvertical, low-resistivity anomalies (Fig. 8), corresponding with major shear zones, represent past conduits and relict pathways, likely formed by the movement of melt and fluids through the crust due to metasomatic mineral alteration from hot magma and/or graphite enrichment (mineralization) along the reactivated shear plane (e.g., Heinson et al., 2006; Comeau

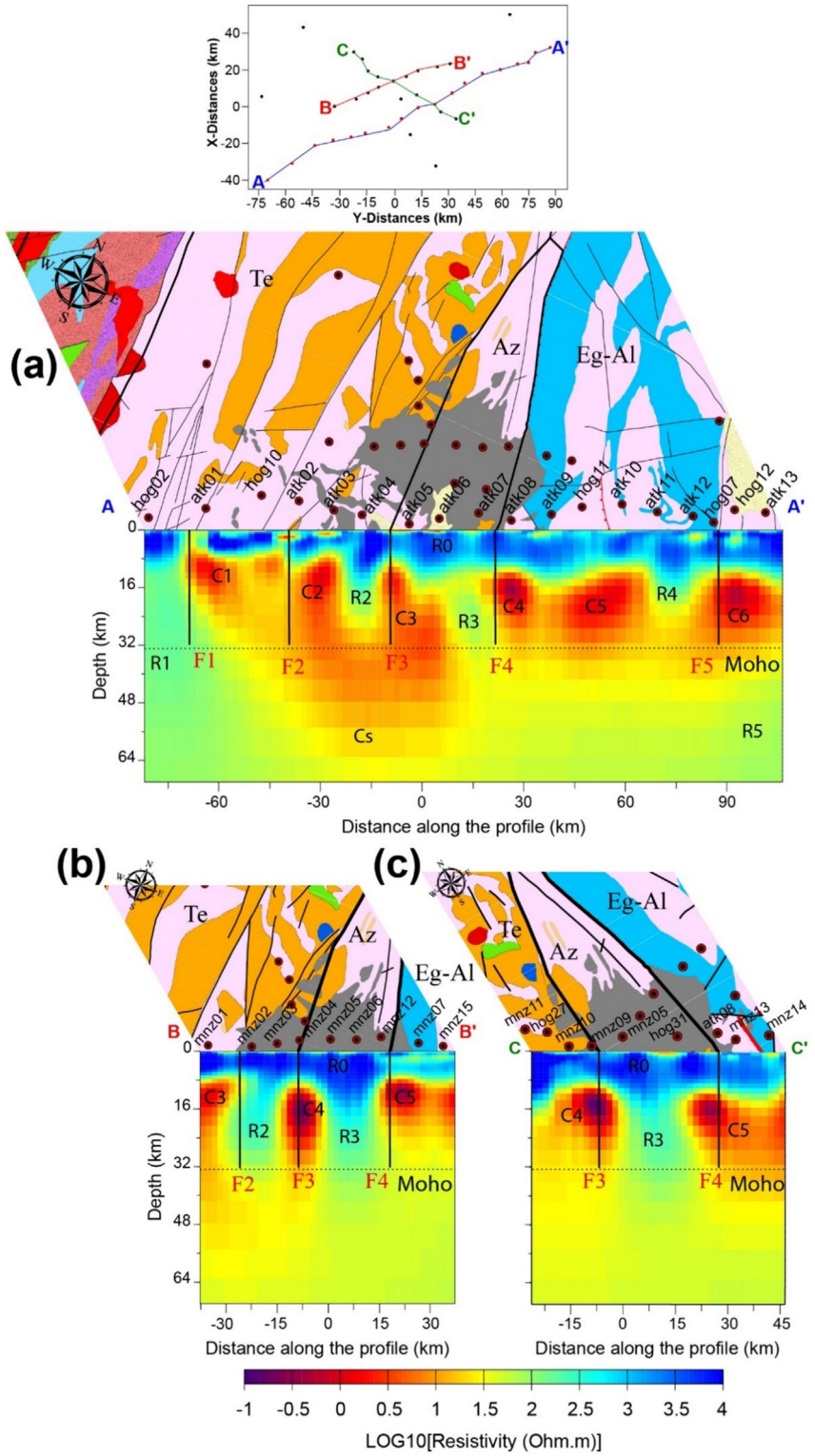

Fig. 8. Vertical cross-sections for the three different profiles extracted from the 3-D electrical resistivity model. The plan-view map at the top shows the locations of measurement sites and the profile lines. Sections are shown along (a) line A-A', (b) line B-B', and (c) line C-C'. Labels C1 to C6 and Cs indicate low-resistivity (conductive) anomalies; labels R1 to R4 indicate moderate-high resistivity anomalies. Labels F3 and F4 mark the projection of the shear zones and terrane boundaries of the Azrou'N'Fad terrane, and labels F1, F2, and F5 mark the projection of other known major lithospheric-scale faults or sutures. These are seen on the geological map shown above the section (plan-view; as in Fig. 3). The abbreviations displayed on the map correspond to the terrane names. Te: Tefedest; Eg-Al: Egéré-Aleksod terrane; Az: Azrou'N'Fad terrane.

et al., 2022b). These conduits may be very narrow or extended linear features, but the physics of the MT technique, the smoothing of the inversion algorithm, and the model cell size may cause them to be imaged as wider features.

5.3. Interpretation of upper mantle electrical resistivity features

Starting at a depth near the base of the crust (>29 km) and extending into the upper mantle (>34 km), the conductive

anomalies discussed above appear to become interconnected and form a horizontal body in the E-W and NE-SW direction (see Fig. 9).

One of the specific features of the Manzaz district is the presence of amphibole that is abundant as microcrysts throughout the volcanic suite, even in the most primitive rocks. Amphibole phenocrysts are observed in mugaearite (kaersutite) from the Atakor region (Azzouni-Sekkal et al., 2007) and in trachyte from the In Tifar neck in the Tazrouk district (fluororichterite) (Azzouni-Sekkal et al., 2013). Benhallou et al. (2016) estimated the equilibrium pressure of amphibole in the Manzaz lavas to be 0.92 GPa for the alkali basalts (with a crystallization temperature of ~1,200 °C), calculated according to the model of Schmidt (1992) (P (±0.6 kbar) = -3.01 + 4.76 Altot). Assuming an average crustal density (e.g., ~2.8 g/cm^3), the depth is estimated (pressure = density*gravity*depth) to be about 33 km, the approximate depth of the crust-mantle boundary. Lucas et al. (2016), using amphibole geobarometry and geothermometry on megacrysts, determined an average temperature of approximately 1,100 °C and a depth of 35 km ± 1 km (given as 0.95 GPa ± 0.03 GPa) for crystallization in the Manzaz volcanic district. This is at the depth of the boundary between the mantle and the continental crust of the LATEA metacraton and is consistent with the obtained electrical resistivity model (Figs. 7 and 8).

Within the lithospheric mantle, a deep sub-circular low-resistivity anomaly (Cs) is imaged in the central part of the model and is located directly beneath the Manzaz and Atakor volcanic districts. To the west (beneath MT stations hog02 and atk01) the lithospheric mantle is noticeably more resistive (R1), with the boundary possibly located along a deep lithospheric fault (labelled F1; Fig. 8). To the east (beneath the MT stations from atk08 to atk13), the lithospheric mantle is also more resistive (R5). The prominent feature Cs may represent the origin of the overlying anomalies. The deep lithospheric fault may be related to its location and emplacement.

The electrical signature from this anomaly is consistent with metasomatism of the sub-continental lithospheric mantle. It is a small-scale and local feature, with a diameter less than 50 km. Reduced electrical resistivity is expected in the areas with the most intense metasomatism (see Jessell et al., 2016; Patko et al., 2021). There is a link between focused metasomatism in the mantle, cumulates near the crust-mantle boundary, and volcanism at the surface (Patko et al., 2021). The low resistivities imaged in this study are compatible with partial melting, possibly generated by decompression melting. Brenna et al. (2018) determined that even small volume monogenetic volcanic cones showed magma with a complex evolution and history in the mantle, before its fast crustal ascent and eruption.

It has been determined (e.g., Dautria et al., 1987; Liégeois et al., 2003, 2005; Kaczmarek et al., 2016) that magma was generated beneath the Hoggar region with emplacement at pressures of 1.0–2.0 GPa or approximately 36–67 km depth (assuming an average density for the crust of ~2.8 g/cm^3 and for the lithospheric mantle of ~3.3 g/cm^3), and that the amphibole-rich xenoliths found in alkali basalts indicated mantle metasomatism, with hydrated minerals (Azzouni-Sekkal et al., 2007). In addition, there is strong evidence for hydrothermal alteration throughout the lithosphere (Benhallou et al., 2016) and the circulation of fluids along major lithospheric faults crossing the Hoggar (Liégeois et al., 2005, 2013). The presence of kaersutite provides more evidence that metasomatic fluids have modified the sub-continental lithospheric mantle (Azzouni-Sekkal et al., 2007). Results obtained on associated nodules, particularly metasomatized clinopyroxene, show that the metasomatic fluids that enriched the lithospheric mantle are either nepheline or melilitic in nature, and are characterized by a HIMU-type isotopic signature, with no EM1-type signature (Beccaluva et al., 2007). The metasomatic process is recent — the Manzaz peridotite nodules show low Sm/Nd ratios but high ^{143}Nd/^{144}Nd ratios (Beccaluva et al., 2007).

5.4. Quantitative constraints on partial melting and saline fluids

Like most Cenozoic lavas in the Hoggar, Manzaz lavas have magnesium number values (Mg# = Mg/[Mg + Fe]) between 0.43 and 0.71 and Zr/Hf ratios between 38 and 49 (Benhallou, 2018). These geochemical indicators help to characterize the source region and point to mantle-derived melts (Benhallou, 2018). Benhallou (2018) estimated partial melting rates of 1–10 % for the lavas of Manzaz. Dautria et al. (1987) predicted ~1–4 % (specifically, 1.2–2.1 % for nephelinite and 3.8–4.4 % for basanite).

We can place constraints on the amount of partial melting from the electrical resistivity measurements. Using a two-phase mixing model (which considers the resistivity of a minor conducting phase and the background rock matrix; see Glover et al., 2000), the volume fraction of a minor conducting phase that is required to explain the electrical resistivity anomalies can be estimated. The empirical relation of Laumonier et al. (2017) can be used to esti-

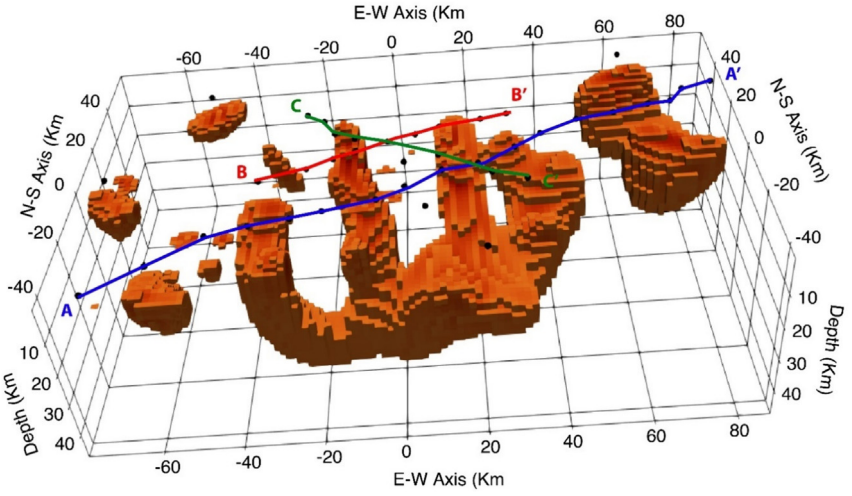

Fig. 9. Iso-surface of ≤ 10 Ωm extracted from the 3-D electrical resistivity model. Coloured lines, A-A', B-B', and C-C', indicate profiles.

mate the electrical resistivity of partial melt, with variations in the pressure–temperature conditions and the water content. Comeau et al (2022a) showed that the models of Laumonier et al. (2017) and Ni et al. (2011) give overlapping results for a pressure of 2 GPa and a water content of 1 wt% (the model of Ni et al., 2011, is only defined for high temperatures and is not extrapolated for other pressures).

It is known that the dissolved water content has a dominant effect on the electrical resistivity of silicic partial melt. In the Manaz district the oxygen fugacity during magma crystallization was higher than that in most intraplate basic magmas (Benhallou et al., 2016), which was probably induced by a significant amount of H_2O dissolved in the magma, and reflected in the systematic presence of amphibole in all rock types at Manzaz. In fact, Benhallou et al. (2016) determined that the magmas in the Manzaz volcanic district had quite high concentrations of water, hypothesizing much more than 2 wt%. Indeed, magmas with high concentrations of alkali elements can dissolve larger amounts of H_2O and CO_2 volatiles (e.g., Samrock et al., 2021, and references therein). Furthermore, alkali ions, namely sodium and potassium ions, act as charge carriers, and therefore when they are more abundant the electrical resistivity is reduced further.

The results show that an anomaly of ~10 Ωm can be explained by 3–10 % partial melt, assuming a water content of 3–6 wt% and a temperature of 1,200 °C (a pressure of 1 GPa corresponds to a depth of ~35 km; see Fig. 10 and the Supplementary Information). In comparison, the results show that a temperature of 1,000 °C means that 10–50 % melt is required to explain the results, which highlights that low-percent melts are feasible only at elevated temperatures and/or greater depths. In comparison, 1–3 % partial melt is required at 1,400 °C.

In addition to partial melts, saline aqueous fluids act to reduce the electrical resistivity. In fact, the combination of a small amount of NaCl-bearing aqueous fluids and a reduced, moderate amount of silicate melt is likely (e.g., Sheng et al., 2023). In fact, Na-rich fluids are known to have interacted with volcanic products in the conduits (shear zones) in Atakor (Cherchali et al., 2022). The experimentally-derived equation from Guo and Keppler (2019) can be used to estimate the electrical resistivity of NaCl-bearing fluids, with variations in the pressure–temperature conditions and the salinity. The results show that saline fluids can be more conductive by a factor of ten or more. An anomaly of ~10 Ωm can be explained by less than 1 % saline fluids. For example, 0.3–1 % saline fluids are required when assuming a salinity of 1–3 wt % and a temperature of 1,200 °C (pressure of 1 GPa corresponds to a depth of ~35 km; see Fig. 10 and Supplementary Information). A salinity for lower crustal fluids of ~6 % has been determined elsewhere (Guo and Keppler, 2019; Patko et al., 2021; Sheng et al., 2023), thus this amount can be considered a minimum. Therefore, hydrothermal alteration, in addition to small amounts of saline fluids, is more likely to be the cause of the crustal resistivity anomalies.

In addition to the partial melt and fluids discussed above, certain mantle minerals can reduce electrical resistivity and help to explain the anomalies, including metasomatism-related phlogopite. Li et al. (2016) computed that 0.1 % phlogopite in peridotite in the upper mantle can produce a bulk resistivity of 10–100 Ωm at temperatures of up to 1,200 °C (see Comeau et al., 2022a). Phlogopite is known in Tahifet lavas (Azzouni-Sekkal et al., 2007; Benhallou, 2000) and even as megacrysts in In Teria (Kaczmarek et al., 2016) and fluorine in the Atakor and Manzaz districts (Azzouni-Sekkal et al., 2007). Fluorine-rich minerals, such as amphibole, if locally concentrated in the upper mantle, can generate regionally high electrical conductivities (Li et al., 2017).

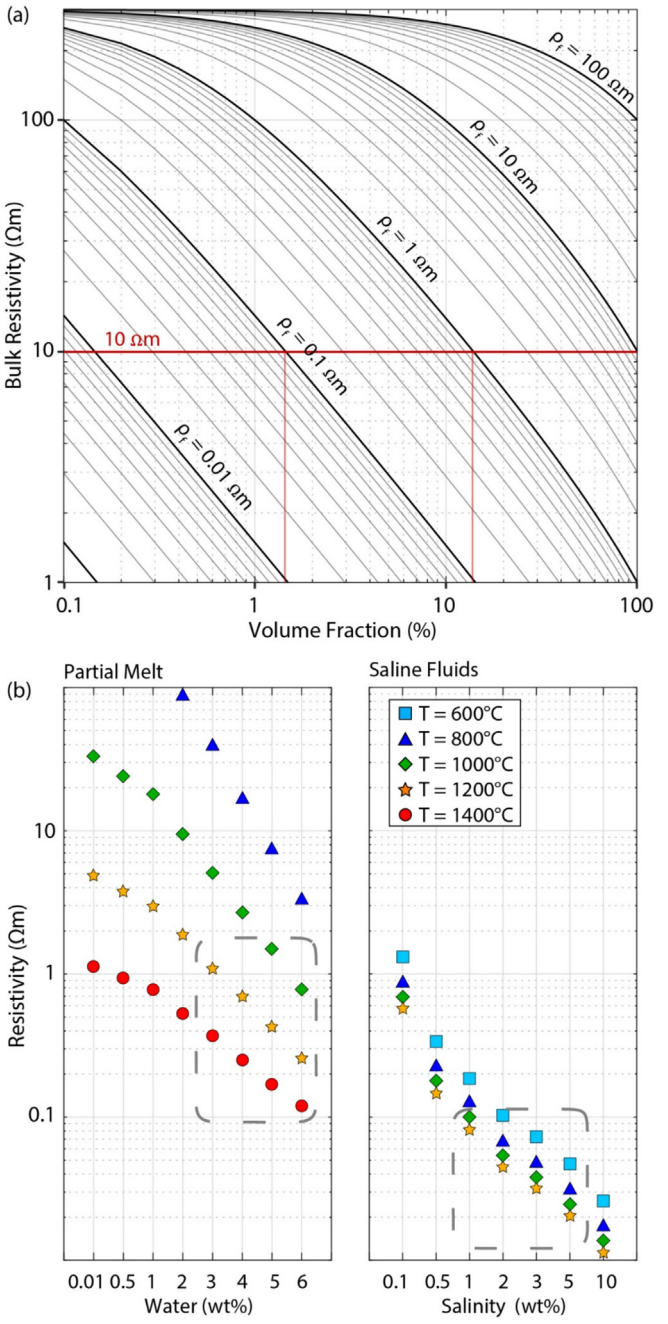

Fig. 10. (a) Bulk resistivity of a two-phase system, as a function of the volume fraction of a minor phase (i.e., conductor). Various resistivities are computed (lines) for the minor phase by using the Hashin-Shtrikman (upper) bound (e.g., Hashin and Shtrikman, 1962; Glover et al., 2000). The major phase, the rock matrix, has a resistivity of 300 Ωm (average background value; the computations are relatively insensitive to this). (b) Estimates for the electrical resistivity of partial melt or saline fluids, based on experimental data. We use the relation from Laumonier et al. (2017) for the resistivity of melt with different temperatures (colours and symbols) and water contents (given as weight-percent H_2O; wt%). We use the relation of Guo and Keppler (2019) for the resistivity of saline fluids with different temperatures (colours and symbols) and salinities (given as weight-percent NaCl). The pressure is set to 1 GPa. The gray boxes denote expected conditions. Note that the horizontal axes are different in both cases and are not to scale.

5.5. Geodynamic implications

The lack of deeper MT signal penetration from the current measurements (1,000–3,000 s periods) and the footprint of the survey area limits the depths that can be imaged reliably. We hypothesize

that the average lithosphere-asthenosphere boundary is below what we can image, for example at a depth of 70–80 km. Therefore, a local, small-scale upwelling feature or features, associated with the mega shear zones, may sit above a broad regional mantle upwelling at greater depths, as has previously been invoked to explain the origin and evolution of this region and the lithospheric bulge associated with the entire Hoggar swell or dome, consistent with other geophysical studies. For example, gravity studies have indicated a large-scale, low-density anomaly on the order of 100+ km depth and 200–400 km in diameter (e.g., Ouadfeul and Aliouane, 2013).

Beccaluva et al., (2007) argue, based on geochemical data, that older cratonic lithospheric mantle was replaced by a passive asthenospheric upwelling. This upwelling could be generated from convection due to a step in lithospheric thickness that occurs between the West African craton to the west and the Hoggar (Beccaluva et al., 2007), or from some other delamination-type scenario (see Stein et al., 2022). The electrical resistivity model is consistent with local lithospheric thinning at reactivated, pre-existing mega shear zones, as proposed by Liégeois et al. (2013), which would produce small-scale, subvertical, linear, narrow low-resistivity anomalies, rather than a single widespread regional feature. Large-scale geophysical measurements have the potential to miss these small-scale features, highlighting the importance of a dense array of measurements (e.g., 5–15 km spacing between measurements in this study, compared to regional studies with 50 km spacing). Liégeois et al. (2013) proposed that the Hoggar Cenozoic volcanism was triggered by the response of the lithosphere to stress at the plate margin: the rigid metacraton with lithospheric-scale shear zones in an intraplate setting allowed mantle melts to rise upwards along reactivated structural weaknesses. Thus, the spatial distribution of volcanism (and mineralization) is controlled by the mega shear zones.

The implications derived here are of interest to other regions. For example, in the Carpathian-Pannonian region there is evidence for a relationship between intracontinental volcanic activity and major structural zones and thus similar mechanisms may exist. In fact, it has been hypothesized that the extraction of long-lived alkaline basaltic partial melts from the mantle occurred along lithospheric-scale shear zones, facilitated by vertical foliation as a response to tectonic compression (Kovács et al., 2020; Koptev et al., 2021; Rubóczki et al., 2024).

6. Conclusion

Continental intraplate volcanic systems, which are located far from plate tectonic boundaries, remain poorly understood. To better understand the origins and mechanisms of intraplate volcanism we use deeply-penetrating geophysical data from magnetotelluric measurements that allows multi-scale imaging of the subsurface architecture from the surface to the lithospheric mantle. This study focuses on the Atakor and Manzaz districts, part of the Central Hoggar Cenozoic volcanic province, Northwest Africa. We generate a three-dimensional electrical resistivity model that crosses multiple terrane domains of the LATEA metacraton and explore the influence of the shear zones on the formation of the volcanic province.

Throughout the crust, the electrical resistivity model reveals narrow, linear conductive features. These lie along terrane boundaries and prominent fault zones (e.g., Azrou N'Fad; trending approximately north–south) and likely reflect the Pan-African mega-shear zones, which were reactivated throughout the tectonic evolution of the region. The model reveals that these faults/sutures zones are lithospheric-scale. The conductive features may be attributed to past fluid flow pathways and mineralization. The results show that these shear zones likely played a significant role in controlling the location of the volcanic activity. This highlights the importance of the tectonic architecture and pre-existing structures for recent Cenozoic volcanic activity.

A deep moderately conductive feature is located in the upper lithospheric mantle directly beneath the Manzaz and Atakor volcanic districts. It is consistent with metasomatism of the subcontinental lithospheric mantle and thus may represent the origin of the fluids responsible for the overlying anomalies. The model is consistent with small-scale, local upwelling features below the linear shear zones, rather than widespread regional lithospheric thinning, although the features may sit atop a regional upwelling associated with the Hoggar swell. Thus, the geophysical model shows remarkable translithospheric images of the subsurface structure of the Central Hoggar, highlighting a mantle melt source and melt pathways related to tectonic architecture, with the results relevant to other regions of continental volcanism.

CRediT authorship contribution statement

Zakaria Boukhalfa: Conceptualization, Data curation, Formal analysis, Investigation, Methodology, Resources, Software, Visualization, Writing – original draft, Writing – review & editing. **Amel Z. Benhallou:** Conceptualization, Funding acquisition, Investigation, Resources, Writing – review & editing. **Matthew J. Comeau:** Formal analysis, Investigation, Methodology, Resources, Software, Visualization, Writing – original draft, Writing – review & editing. **Abderrezak Bouzid:** Conceptualization, Funding acquisition, Investigation, Resources, Writing – review & editing. **Abderrahmane Bendaoud:** Conceptualization, Writing – review & editing. **Aboubakr Deramchi:** Investigation.

Declaration of competing interest

The authors declare that they have no known competing financial interests or personal relationships that could have appeared to influence the work reported in this paper.

Acknowledgements

This work is part of the Hoggar geodynamics project based at CRAAG, entitled: "Precambrian and Phanerozoic geodynamics of the Hoggar lithosphere based on geological and magnetotelluric data". The data used in this paper come from various field surveys conducted with support from CRAAG and USTHB. We express our sincere gratitude to both institutions for their invaluable support and assistance provided during the process that led to the completion of field work. Additionally, we extend our thanks to all those who took part in data collection during the various field surveys. Furthermore, we acknowledge the authorities of the province of Tamanrasset for their help in carrying out the field surveys. The authors are thankful for comments from the Associate Editor, two anonymous reviewers, and J.-P. Liégeois.

Appendix A. Supplementary material

Supplementary data to this article can be found online at https://doi.org/10.1016/j.gr.2024.08.003.

References

Aïdrous-Belhocine, K., 2010. Étude pétrologique des granitoïdes Panafricains de la partie Nord du Bloc Azrou-n'Fad (Région du col d'Azrou et du Manzaz) Hoggar Central, Algérie. USTHB, FSTGAT, Algiers, Algeria. *Thesis*.

Aït-Hamou, F., 2000. Un exemple de "point chaud" intracontinental en contexte de plaque quasi-stationnaire : étude pétrologique et géochimique du Djebel Taharaq et évolution du volcanisme cénozoïque de l'Ahaggar (Sahara algérien). Montpellier, France, Thesis. http://www.theses.fr/2000MON20074.

Aït-Hamou, F., Dautria, J.M., 1994. Le magmatisme Cénozoïque du Hoggar : une synthèse des données disponibles. Mise au point sur l'hypothèse d'un point chaud. Bull. Serv. Géol. De L'alg 5 (1), 49–68.

Aït-Hamou, F., Dautria, J., 1997. Spatiotemporal and compositional variations of the Cenozoic Volcanism in the Ahaggar area: evidence for a hot spot in relation with the African Plate motion. Terra Nova 9 (9), 62–66.

Aït-Hamou, F., Dautria, J.M., Cantagrel, J.M., Dostal, J., Briqueu, L., 2000. Nouvelles données géochronologiques et isotopiques sur le volcanisme cénozoïque de l'Ahaggar (Sahara algérien):des arguments en faveur de l'existenced'un panache. Comptes Rendus De l Académie Des Sciences - Series IIA - Earth and Planetary Science 330 (12), 829–836. https://doi.org/10.1016/S1251-8050(00)00217-2.

Aloui, T., Dasgupta, P., Chaabani, F., 2012. Facies pattern of the Sidi Aïch Formation: Reconstruction of Barremian paleogeography of Central North Africa. Journal of African Earth Sciences 71–72, 18–42. https://doi.org/10.1016/j.jafrearsci.2012.06.004.

Ayadi, A., Dorbath, C., Lesquer, A., Bezzeghoud, M., 2000. Crustal and upper mantle velocity structure of the Hoggar swell (central Sahara, Algeria). Phys. Earth Planet. Inter. 118, 111–123. https://doi.org/10.1016/S0031-9201(99)00134-X.

Azzouni-Sekkal, A., Liégeois, J.P., Bechiri-Benmerzoug, F., Belaidi-Zinet, S., Bonin, B., 2003. The "Taourirt" magmatic province, a marker of the very end of the Pan-African orogeny in the Tuareg Shield: review of the available data and Sr-Nd isotope evidence. J. Afr. Earth Sci. 37, 331–350. https://doi.org/10.1016/S0031-9201(99)00134-X.

Azzouni-Sekkal, A., Bonin, B., Benhallou, A., Yahiaoui, R., Liégeois, J.P., 2007. Cénozoïque alkaline volcanism of Atakor massif, Hoggar, Algeria. in Cenozoic Volcanism in the Mediterranean Area, 418, 321-340, eds Beccaluva,L., Bianchini, G.,Wilson, M. *Geol. Soc. Am. Spec. Pap.* DOI: 10.1130/2007.2418(16).

Azzouni-Sekkal, A., Bonin, B., Ben El Khaznadji, R., 2013. Occurrence of fluororichterite and fluorian biotite in the In Tifar trachyte neck (Tazrouk district, Hoggar volcanic province, Sahara, Algeria). J. Afr. Earth Sci. 85, 1–11. https://doi.org/10.1016/j.jafrearsci.2013.04.003.

Baudin, P., 1986. Magmatisme mésozoïque du fossé de la Bénoué (Nigéria). Caractéristiques pétrologiques et géochimiques, signification géodynamique. Aix-Marseille, France. Thesis.

Béa, A., 1987. Grabens et volcanisme tholeiitique continental associé d'âge Odovinien-Dévonien probable, dans la région de Garoua au Nord-Cameroun. Aix-Marseille, France, *Thesis*.

Beccaluva, L., A., Azzouni-Sekkal, A., Benhallou, G., Bianchini, R., M., Ellam, M., Marzola, F., Siena F.M. Stuart, 2007. Intracratonic asthenosphere up welling and lithosphere rejuvenation beneath the Hoggar swell (Algeria): Evidence from HIMU metasomatised lherzolite mantle xenoliths. *Earth Planet. Sci. Lett.*, 260(3-4), 482-494. DOI: 10.1016/j.epsl.2007.05.047.

Ben El Khaznadji, R., Azzouni-Sekkal, A., Benhallou, A., Liégeois, J.P., Bernard, B., 2017. Neogene felsic volcanic rocks in the Hoggar province: volcanology, geochemistry and age of the Azrou trachyte-phonolite association (Algerian Sahara). J. Afr. Earth Sci 127, 222–234. https://doi.org/10.1016/j.jafrearsci.2016.07.013.

Benhallou, A.Z., 2000. Étude du volcanisme alcalin cénozoïque de la région de Tahifet (Bloc d'Azrou N'Fad, Hoggar central, Algérie). USTHB-FSTGAT, Algiers, Algeria. Thesis.

Benhallou, A., 2018. Contribution à la connaissance du manteau Hoggarien, par l'étude des laves alcalines cénozoïques du massif du Manzaz. USTHB-FSTGAT, Algiers, Algeria. *Thesis.*

Benhallou, A.-Z., Azzouni-Sekkal, A., Bonin, B., Ikhlef Debabha, F., Ben El Khaznadji, R., Liégeois, J.-P., 2016. Le district volcanique du Manzaz (Hoggar, Sahara algérien): Géologie, pétrographie et minéralogie. Bull. Serv. Géol. De L'alg 27 (1–2) https://www.asjp.cerist.dz/en/article/38488.

Benhallou A.Z., Megueni, Y., Boussisse, F., Debabha, F.I., Babkar, Y., Boukhalfa, Z., Aghanbilou, K., Azzouni-Sekkal, A., Dautria, J.M., Bodinier, J.L., 2019. The South West Atakor Volcanic District (Hoggar-Algeria): Petrography and Mineralogy from the Taessa Lavas. In: Doronzo, D., Schingaro, E., Armstrong-Altrin, J., Zoheir, B. (eds) Petrogenesis and Exploration of the Earth's Interior. CAJG 2018. Advances in Science, Technology & Innovation (ASTI). Springer, Cham. DOI: 10.1007/978-3-030-01575-6_7.

Benmessaoud, M., 2014. Recherches sur l'Acheuléen de l'Ahaggar : Les matières premières lithiques; l'outillage lithique, rapport éclats/outil; le cadre stratigraphique et chronologique. Exemple du site Téhéntawek. Université de Paris, France. Thesis.

Bertrand, J.M., Caby, R., 1977. Carte géologique du Hoggar, Algerie, Direction des Mines et de la Géologie, SONAREM, scale 1:1,000,000.

Bertrand, E. et al., 2012. Magnetotelluric imaging of upper-crustal convection plumes beneath the Taupo Volcanic Zone, New Zealand. Geophys. Res. Lett. 39 (2). https://doi.org/10.1029/2011GL050177.

Bibby, H.M., Caldwell, T.G., Brown, C., 2005. Determinable and non-determinable parameters of galvanic distortion in magnetotellurics. Geophys. J. Int. 163 (3), 915–930. https://doi.org/10.1111/j.1365-246X.2005.02779.x.

Black, R., 1984. The Pan-African event in the geological framework of Africa. Pangea 2, 8–16.

Black, R., Latouche, L., Liégeois, J.P., Caby, R., Bertrand, J.M., 1994. Pan- African displaced terranes in the Tuareg shield (central Sahara). Geology 22, 641–644.

Boissonnas, J. 1973. Les granites à structures concentriques et quelques autres granites tardifs de la chaîne panafricaine en Ahaggar (Sahara central, Algérie). Paris, Mém. CRZA, serv. Géol. no. 16, et Mem. H.S. BRGM, (coed.) CNRS-BRGM 1974, 2 vol., 662 pp.

Booker, J., 2014. The magnetotelluric phases tensor: a critical review. Surv Geophys. 35, 7–40. https://doi.org/10.1007/s10712-013-9234-2.

Boubekri, H., Hamoudi, M., Bendaoud, A., Priezzhev, I., Allek, K., 2015. 3D structural cartography based on magnetic and gravity data inversion–Case of South-West Algeria. J. Afr. Earth Sci 112, 471–484. https://doi.org/10.1016/j.jafrearsci.2015.02.001.

Boukhalfa, Z., Bouzid, A., Xu, Y., Bendaoud, A., Yang, B., Hamoudi, M., Djeddi, M., 2020. Magnetotelluric investigation of the Precambrian crust and intraplate Cenozoic volcanism in the Gour Oumelalen area, Central Hoggar. South Algeria. *Geophys J Int* 223 (3), 1973–1986. https://doi.org/10.1093/gji/ggaa432.

Bournas, N., Galdeano, A., Hamoudi, M., Baker, H., 2003. Interpretation of the aeromagnetic map of Eastern Hoggar (Algeria) using the Euler deconvolution, analytic signal and local wavenumber methods. J. Afr. Earth Sci. 37, 191e205. https://doi.org/10.1016/j.jafrearsci.2002.12.001.

Bouzid, A. *et al.*, 2015. Lithospheric structure of the Atakor metacratonic volcanic swell (Hoggar, Tuareg Shield, southern Algeria): electrical constraints from magnetotelluric data, in *The Interdisciplinary Earth: A Volume in Honor of Don L. Anderson,* Vol. **514,** pp. 239–255, eds Foulger, G.R., Lustrino, M. & King, S.D., *Geol. Soc. Am. Spec. Pap.* DOI: 10.1130/2015.2514(15).

Bouzid, A., Akacem, N., Hamoudi, M., Ouzegane, K., Abtout, A., Kienast, J.-R., 2008. Modélisation magnétotellurique de la structure géologique profonde de l'unité granulitique de l'In Ouzzal (Hoggar occidental). Compt. Rend. Geosci. 340, 711–722. https://doi.org/10.1016/j.crte.2008.08.001.

Brahimi, S., Liégeois, J.P., Ghienne, J.F., Munschy, M., Bourmatte, A., 2018. The Tuareg shield terranes revisited and extended towards the northern Gondwana margin: Magnetic and gravimetric constraints. Earth Sci. Rev. 185, 572–599. https://doi.org/10.1016/j.earscirev.2018.07.002.

Brenna, M., Cronin, S.J., Smith, I.E.M., Tollan, P.M.E., 2018. Olivine xenocryst diffusion reveals rapid monogenetic basaltic magma ascent following complex storage at Pupuke Maar, Auckland Volcanic Field, New Zealand. *Earth Planet. Sci. Lett.,* 499, 13–22. DOI: 10.1016 /j.epsl.2018.07.015.

Brown, C., Girdler, R.W., 1980. Interpretation of african gravity and its implication for the breakup of the continents. J. Geophys. Res. 85, 6443–6455. https://doi.org/10.1029/JB085iB11p06443.

Caldwell, T.G., Bibby, H.M., Brown, C., 2004. The magnetotelluric phase tensor. Geophys. J. Inter. 158 (2), 457–469. https://doi.org/10.1111/j.1365-246X.2004.02281.x.

Cashman, K.V., Sparks, R.S.J., 2013. How volcanoes work: A 25 year perspective. Geol. Soc. Am. Bull. 125 (5–6), 664–690. https://doi.org/10.1130/B30720.1.

Cheilletz, A., Bertrand, J.M., Charoy, B., Moulahoum, O., Bouabsa, L., Farrar, E., Zimmerman, J.L., Dautel, D., Archibald, D.A., Boullier, A.M., 1992. Géochimie et géochronologie Rb/Sr, K/Ar, 40Ar/39Ar des complexes granitiques panafricains de la région de Tamanrasset (Algérie): Relation avec les minéralisations Sn -W associées et l'évolution tectonique du Hoggar central. *Bull. Soc. Géol.Fr.* 163, 733–750.

Cherchali, M.E.H., Liégeois, J.P., Mesbah, M., Daas, N., Amrous, K., Ouarezki, S.A., 2022. Central Hoggar groundwaters and the role of shear zones: $^{87}Sr/^{86}Sr$, $\delta^{18}O$, $\delta^{2}H$ and ^{14}C isotopes, geochemistry and water-rock interactions. Appl Geochem 137. https://doi.org/10.1016/j.apgeochem.2021.105179.

Choubert, G., Faure-Muret, A., 1975. Atlas géologique du monde 1: 10000000: Afrique. *Comm. Carte Geol. Monde*, Unesco, Paris. Feuilles 6, 7, 8.

Comeau, M.J., Becken, M., Käufl, J., Grayver, A., Kuvshinov, A., Tserendug, S., Batmagnai, E., Demberel, S., 2020a. Evidence for terrane boundaries and suture zones across Southern Mongolia detected with a 2-dimensional magnetotelluric transect. Earth, Planets Space 72 (5). https://doi.org/10.1186/s40623-020-1131-6.

Comeau, M.J., Becken, M., Connolly, J.A.D., Grayver, A.V., Kuvshinov, A.V., 2020b. Compaction-driven fluid localization as an explanation for lower crustal electrical conductors in an intracontinental setting. Geophys Res Lett 47. https://doi.org/10.1029/2020GL088455.

Comeau, M.J., Becken, M., Kuvshinov, A.V., 2022a. Imaging the whole-lithosphere architecture of a mineral system—Geophysical signatures of the sources and pathways of ore-forming fluids. Geochem, Geophys Geosyst 23. https://doi.org/10.1029/2022GC010379.

Comeau, M.J., Becken, M., Grayver, A.V., Käufl, J., Kuvshinov, A., 2022b. The geophysical signature of a continental intraplate volcanic system: From surface to mantle source. Earth Planet Sci Lett 587. https://doi.org/10.1016/j.epsl.2021.117307.

Conrad, C.P., Bianco, T.A., Smith, E.I., Wessel, P., 2011. Patterns of intraplate volcanism controlled by asthenospheric shear. Nat. Geosci. 4, 317–321. https://doi.org/10.1038/ngeo1111.

Courtillot, V., Davaille, A., Besse, J., Stock, J., 2003. Three distinct types of hotspots in he Earth's mantle. Earth Planet Sci Lett 205, 295–308. https://doi.org/10.1016/S0012-821X(02)01048-8.

Daly, M.C., 1988. Crustal shear zones in central africa: A kinematic approach to proterozoic tectonics. Episodes J. Int. Geosci 11, 5–11. https://doi.org/10.18814/epiiugs/1988/v11i1/003.

Dautria, J.M., Liotard, J.M., Cabanes, N., et al., 1987. Amphibole-rich xenoliths and host alkali basalts: petrogenetic constraints and implications on the recent evolution of the upper mantle beneath Ahaggar (Central Sahara, Southern Algeria). Contr. Mineral. Petrol 95, 133. https://doi.org/10.1007/BF00381263.

Dautria, J.M., Dostal, J., Dupuy, C., Liotard, J.M., 1988. Geochemistry and petrogenesis of alkali basalts from Tahalra (Hoggar, Northwest Africa). Chem. Geol. 69, 17–35. https://doi.org/10.1016/0009-2541(88)90155-6.

Decker, R., Decker, B., 2005. Volcanoes. W.H. Freeman & Co, New York, p. 326.

Deramchi, A., Bouzid, A., Bendaoud, A., Ritter, O., Hamoudi, M., Cruces-Zabala, J., Meqbel, N., Boukhalfa, Z., Boughchiche, S.S., Abtout, A., Boukhlouf, W., Bendekken, A., 2020. Neoproterozoic amalgamation and Phanerozoic reactivation of Central/ Western Hoggar (Southern Algeria, Tuareg Shield) lithosphere imaging using Magnetotelluric data. *J. Geodyn.* DOI: 10.1016/j.jog.2020.101764.

Deramchi, A., Vauchez, A., Bendaoud, A., Caxito, F.A., Boukhalfa, Z., Doukkari, S., Maouche, S., Lana, C., Aghanbilou, K., Bouzid, A., 2023. Polyphase deformation and deformation-magmatism interaction in the Pan-African 4°50′ shear zone (Hoggar, Southern Algeria). Precambrian Res 393. https://doi.org/10.1016/j.precamres.2023.107085.

Derder, M.E.M., Maouche, S., Missenard, Y., et al., 2023. Upper Cretaceous Cenozoic uplifts and tectonics within a Precambrian shield — insight from the Hoggar (Algeria) local sedimentary cover. Arab. J. Geosci. 16, 650. https://doi.org/10.1007/s12517-023-11761-y.

Egbert, G., Kelbert, A., 2012. Computational recipes for electromagnetic inverse problems. Geophys. J. Inter. 189, 251–267. https://doi.org/10.1111/j.1365-246X.2011.05347.x.

Fishwick, S., Bastow, I.D., 2011. Towards a better understanding of African topography: a review of passive-source seismic studies of the African crust and upper mantle. Geol Soc, Spec. Pub 357 (1), 343–371. https://doi.org/10.1144/SP357.19.

Franz, G., Pudlo, D., Urlacher, G., Haußmann, U., Boven, A., Wemmer, K., 1994. The Darfur Dome, western Sudan: the product of a subcontinental mantle plume. Geol. Rundsch. 83, 614–623.

Gangopadhyay, A., Pulliam, J., Sen, M.-K., 2007. Waveform modeling of teleseismic S, Sp, SsPmP, and shear-coupled PL waves for crust- and upper-mantle velocity structure beneath Africa. Geophys. J. Inter. 170 (3), 1210–1226. https://doi.org/10.1111/j.1365-246X.2007.03470.x.

Girod, M., 1971. Le massif volcanique de l'Atakor (Hoggar, Sahara algérien). *Mém. CRZA, Sér. Géol.*, 12, 155 p. ed. C N R S, Paris.

Glover, P.W.J., Hole, M.J., Pous, J., 2000. A modified Archie's law for two-conducting phases. Earth Planet. Sci. Lett. 180, 369–383. https://doi.org/10.1016/S0012-821X(00)00168-0.

Guo, H., Keppler, H., 2019. Electrical Conductivity of NaCl-Bearing Aqueous Fluids to 900 °C and 5 GPa. J. Geophys. Res. Solid Earth 124 (2), 1397–1411. https://doi.org/10.1029/2018JB016658.

Harris, N., Hunt, A., Parkinson, I., Tindle, A., Yondon, M., Hammond, S., 2010. Tectonic implications of garnet-bearing mantle xenoliths exhumed by Quaternary magmatism in the Hangay dome, central Mongolia. Contrib. Mineral. Petrol. 160, 67–81. https://doi.org/10.1007/s00410-009-0466-6.

Harrouchi, L., Hamoudi, M., Bendaoud, A., Beguiret, L., 2016. Application of 3D Euler deconvolution and improved tilt angle to the aeromagnetic data of In Ouzzal terrane, western Hoggar. Algeria. *Arab. J. Geosci* 9 (7), 508. https://doi.org/10.1007/s12517-016-2536-1.

Harrouchi, L., Berguig, M.C., Boutrika, R., Hamoudi, M., Bendaoud, A., 2020. Application of Riesz Transform to the aeromagnetic data of the central In Ouzzal terrane and adjacent zone, southern Algeria. Boll. Di Geofis. Teor Ed Applicata 61 (4), 487–498. https://doi.org/10.4430/bgta0334.

Hashin, Z., Shtrikman, S., 1962. A variational approach to the theory of the effective magnetic permeability of multiphase materials. J. Appl. Phys. 33, 3125–3131. https://doi.org/10.1063/1.1728579.

Heinson, G.S., Direen, N.G., Gill, R.M., 2006. Magnetotelluric evidence for a deep-crustal mineralizing system beneath the Olympic Dam iron oxide copper-gold deposit, southern Australia. Geology 34, 573–576. https://doi.org/10.1130/G22222.1.

Jessell, M.W., Begg, G.C., Miller, M.S., 2016. The geophysical signatures of the West African Craton. Precambrian Research 274, 3–24. https://doi.org/10.1016/j.precamres.2015.08.010.

Jin, S., Sheng, Y., Comeau, M.J., Becken, M., Wei, W., Ye, G., Zhang, L.T., Dong, H., 2022. Relationship of the crustal structure, rheology, and tectonic dynamics beneath the Lhasa-Gangdese terrane (southern Tibet) based on a 3-D electrical model. J. Geophys. Res. Solid Earth 127. https://doi.org/10.1029/2022JB024318.

Jones, A.G., 1992. Electrical conductivity of the continental lower crust. In: Fountain, D.M., Acrulus, R.J., Kay, R.W. (Eds.), Continental Lower Crust. Elsevier, New York, pp. 81–143.

Kaczmarek, M.-A., Bodinier, J.-L., Bosch, D., Tommasi, A., Dautria, J.-M., Kechid, S.A., 2016. Metasomatized Mantle Xenoliths as a Record of the Lithospheric Mantle Evolution of the Northern Edge of the Ahaggar Swell, In Teria (Algeria). J. Petrol 57 (2), 345–382. https://doi.org/10.1093/petrology/egw009.

Käufl, J.S., Grayver, A.V., Comeau, M.J., Kuvshinov, A., Becken, M., Kamm, J., Batmagnai, E., Demberel, S., 2020. Magnetotelluric multiscale 3-D inversion reveals crustal and upper mantle structure beneath the Hangai and Gobi-Altai region in Mongolia. Geophys. J. Inter 221 (2), 1002–1028. https://doi.org/10.1093/gji/ggaa039.

King, S.D., Anderson, D.L., 1998. Edge-driven convection. Earth Planet. Sci. Lett. 160 (3–4), 289–296. https://doi.org/10.1016/S0012-821X(98)00089-2.

Kirkby, A.L., Zhang, F., Peacock, J., Hassan, R., Duan, J., 2019. The MTPy software package for magnetotelluric data analysis and visualisation. Journal of Open Source Software 4 (37), 1358. https://doi.org/10.21105/joss.01358.

Koptev, A., Cloetingh, S., Kovács, I.J., et al., 2021. Controls by rheological structure of the lithosphere on the temporal volution of continental magmatism: inferences from the Pannonian Basin system. Earth Planet. Sci. Lett. 565. https://doi.org/10.1016/j.epsl.2021.116925.

Kovács, I. et al., 2020. The role of water and compression in the genesis of alkaline basalts: inferences from the Carpathian-Pannonian. Lithos 354–355. https://doi.org/10.1016/j.lithos.2019.105323.

Krieger, L., Peacock, J., 2014. MTpy: A Python toolbox for magnetotellurics. Computers and Geosciences 72, 167–175. https://doi.org/10.1016/j.cageo.2014.07.013.

Lasserre, M., Baubron, J.C., Cantagrel, J.M., 1977. Existence d'une couverture non plissée d'âge paleozoïque inferieur au sein de la zone mobile de l'Afrique centrale : Age K/Ar des formations de type Mangbai. *C. R. Acad. Sci.* Paris, D 284, 2667–2670.

Laumonier, M., Gaillard, F., Muir, D., Blundy, J., Unsworth, M., 2017. Giant magmatic water reservoirs at mid-crustal depth inferred from electrical conductivity and the growth of the continental crust. Earth Planet. Sci. Lett. 457, 173–180. https://doi.org/10.1016/j.epsl.2016.10.023.

Le Bas, M.J., Le Maitre, R.W., Streckeisen, A., Zanettin, B., 1986. A chemical classification of volcanic rocks based on the total alkali–silica diagram. Journal of Petrology 27 (3), 745–750. https://doi.org/10.1093/petrology/27.3.745.

Le Bas, M.J., Le Maitre, R.W., Woolley, A.R., 1992. The construction of the total alkali–silica chemical classification of volcanic rocks. Mineralogy and Petrology 46, 1–22. https://doi.org/10.1007/BF01160698.

Le Maitre, R.W., ed., 2002. Igneous Rocks: A Classification and Glossary of Terms (2nd edition): Recommendations of the International Union of Geosciences Subcommission on the Systematics of Igneous Rocks: Cambridge, Cambridge University Press, 236 p. DOI: 10.1017/CBO9780511535581.

Le Maitre, R.W. et al., 1989. A classification of igneous rocks and glossary of terms. Blackwell, Oxford.

Lemnifi, A.A., Liu, L., Browning, J., 2020. Lithospheric layering beneath northern Central Africa by S-to-P receiver functions. J. Afr. Earth 166. https://doi.org/10.1016/j.jafrearsci.2020.103827.

Lesquer, A., Bourmatte, A., Dautria, J.M., 1988. Deep structure of the Hoggar domal uplift (Central Sahara, south Algeria) from gravity, thermal and petrological data. Tectonophysics 152, 71–87. https://doi.org/10.1016/0040-1951(88)90030-3.

Lesquer, A., Bourmatte, A., Ly, S., Lesquer, J.M., 1989. First heat flow determination from the Central Sahara: Relationship with the Pan-African belt and Hoggar domal uplift. J. Afr. Earth Sci. 9, 41–48. https://doi.org/10.1016/0899-5362(89)90006-7.

Lesquer, A., Takherist, D., Dautria, J.M., Hadiouche, O., 1990. Geophysical and petrological evidence for the presence of an "anomalous" upper mantle beneath the Sahara basins (Algeria). Earth Planet. Sci. Lett. 96 (3–4), 407–418. https://doi.org/10.1016/0012-821X(90)90016-Q.

Liégeois, J.P., 2019. A New Synthetic Geological Map of the Tuareg Shield: An Overview of Its Global Structure and Geological Evolution. In: Bendaoud, A., Hamimi, Z., Hamoudi, M., Djemai, S., Zoheir, B. (Eds.), The Geology of the Arab World--an Overview. Springer Geology. Springer, Cham. https://doi.org/10.1007/978-3-319-96794-3_2.

Liégeois, J.P., Latouche, L., Boughrara, M., Navez, J., Guiraud, M., 2003. The LATEA metacraton (Central Hoggar, Tuareg shield, Algeria): Behaviour of an old passive margin during the Pan-African orogeny. J. Afr. Earth Sci. 37, 161–190. https://doi.org/10.1016/j.jafrearsci.2003.05.004.

Liégeois, J.P., Benhallou, A., Azzouni-Sekkal, A., Yahiaoui, R., Bonin, B., 2005. The Hoggar swell and volcanism: reactivation of the Precambrian Tuareg shield during Alpine convergence and West African Cenozoic volcanism, in *Plates, Plumes and Paradigms,* 388, 379–400, eds Foulger, G.R., Natland, J.H., Presnall, D. C., Anderson, D.L., *Geol. Soc. Am*. Spec. Pap. DOI: 10.1130/0-8137-2388-4.379.

Liégeois, J.P., Abdelsalam, M.G., Ennih, N., Ouabadi, A., 2013. Metacraton: nature, genesis and behavior. Gondwana Res. 23 (1), 220–237. https://doi.org/10.1016/j.gr.2012.02.016.

Li, Y., Yang, X., Yu, J.-H., Cai, Y.-F., 2016. Unusually high electrical conductivity of phlogopite: The possible role of fluorine and geophysical implications. Contrib. Mineral. Petrol 171 (4), 37. https://doi.org/10.1007/s00410-016-1252-x.

Li, Y., Jiang, H.T., Yang, X.Z., 2017. Fluorine follows water: Effect on electrical conductivity of silicate minerals by experimental constraints from phlogopite. Geochim Cosmochim Acta 217, 16–27. https://doi.org/10.1016/j.gca.2017.08.020.

Liu, H.L., Gao, S.S., 2010. Spatial variations of crustal characteristics beneath the Hoggar swell, Algeria, revealed by systematic analyses of receiver functions from a single seismic station. Geochem. Geophys. Geosy. 11 (8), 1–14. https://doi.org/10.1029/2010GC003091.

Lucas, C., Benhallou, A.Z., Azzouni-Sekkal, A., Bonin, B., Bechiri-Benmerzoug, F., 2014. Mégacristaux D'origine Profonde Dans Les Tephra Du District Volcanique Du Manzaz (Hoggar Central, Saharien Algérien). *Colloque national sur la géologie et les ressources minérales du Hoggar*. USTHB/FSTGAT, Algiers, Algeria.

Lucas, C., Benhallou, A., Bonin, B., Azzouni-Sekkal, A., Bechiri-Benmerzoug, F., 2016. Megacrysts in Tephra of the Manzaz Volcanic District (Central Hoggar, Algerian Sahara). *Presented at Friedländer Workshop in volcanology on Probing Magma Reservoirs in Time and Space*. DOI: 10.13140/RG.2.2.32514.99526.

Meert, J.G., Lieberman, B.S., 2008. The Neoproterozoic assembly of Gondwana and its relationship to the Ediacaran-Cambrian radiation. Gondwana Res. 14, 5–21. https://doi.org/10.1016/j.gr.2007.06.007.

Megueni, Y., Boussisse, I.F., 2017. Etude pétrographique et minéralogique des basaltes alcalins de la région de Taessa, Hoggar, 120p. USTHB-FSTGAT, Algiers, Algeria.

Meqbel, N., 2009. The Electrical Conductivity Structure of the Dead Sea Basin Derived from 2-D and 3-D Inversion of Magnetotelluric Data. Freie Univ, Berlin, Germany. Thesis.

Mougenot, D., Recq, M., Virlogeux, P., Lepvrier, C., 1986. Seaward extension of the East African Rift. Nature 321, 599–603. https://doi.org/10.1038/321599a0.

Ni, H., Keppler, H., Behrens, H., 2011. Electrical conductivity of hydrous basaltic melts: Implications for partial melting in the upper mantle. Contrib Mineral Petrol 162 (3), 637–650. https://doi.org/10.1007/s00410-011-0617-4.

Ostos, L., Park, S.K., 2012. Foundering lithosphere imaged with magnetotelluric data beneath Yosemite National Park, California. Geosphere 8, 98–104. https://doi.org/10.1130/GES00657.1.

Ouadfeul, S.A., Aliouane, L., 2013. Structural edges delimitation from gravity data using the wavelet transform. Symposium on the Application of Geophysics to Engineering and Environmental Problems Proceedings 403–410. https://doi.org/10.4133/sageep2013-142.1.

Ouattara, Y., Zigone, D., Maggi, A., 2019. Rayleigh wave group velocity dispersion tomography of West Africa using regional earthquakes and ambient seismic noise. J Seismolog 23, 1201–1221. https://doi.org/10.1007/s10950-019-09860-z.

Paquette, J.L., Caby, R., Djouadi, M.T., Bouchez, J.L., 1998. U-Pb dating of the end of the Pan-African orogeny in the Tuareg sheild: the post-collisional syn-shear Tiouein pluton (Western Hoggar, Algeria). Lithos 45, 245–254.

Parkinson, W.D., 1962. The influence of continents and oceans on geomagnetic variations. Geophysical Journal International 2, 441–449. https://doi.org/10.1111/j.1365-246X.1962.tb02992.x.

Patko, L., Novak, A., Klebesz, R., Liptai, N., Lange, T.P., Molnar, G., et al., 2021. Effect of metasomatism on the electrical resistivity of the lithospheric mantle–an integrated research using magnetotelluric sounding and xenoliths beneath the Nógrád-Gömör Volcanic Field. Global Planet. Change 197. https://doi.org/10.1016/j.gloplacha.2020.103389.

Popoff, M., 1988. Du Gondwana à l'atlantique sud: les connexions du fossé de la bénoué avec les bassins du Nord-Est brésilien jusqu'à l'ouverture du golfe de Guinée au crétacé inférieur. J. Afr. Earth Sci. Spec. Publ. 7, 409–431. https://doi.org/10.1016/0899-5362(88)90086-3.

Popoff, M., Kampunzu A.B., Coulon C., Esquevin J., 1982 – Découverte d'un volcanisme mésozoïque dans le Nord-est du Nigéria : datations absolues, caractères magmatiques et signification géodynamique dans l'évolution du rift de la Bénoué. In : Rifts et fossés anciens, résumé, *Trav. Lab. Sci. Terre*, Marseille, St Jérôme, 19, pp 449 – 478.

Raddick, M.J., Parmentier, E.M., Scheirer, D.S., 2002. Buoyant decompression melting: A possible mechanism for intraplate volcanism. J. Geophys. Res. 107 (B10), 2228. https://doi.org/10.1029/2001JB000617.

Roberts, G.G., White, N., 2010. Estimating uplift rate histories from river profiles using African examples. J. Geophys. Res. 115, B02406. https://doi.org/10.1029/2009JB006692.

Robertson, K., Thiel, S., Meqbel, N., 2020. Quality over quantity: on workflow and model space exploration of 3D inversion of MT data. Earth Planets Space 72 (2). https://doi.org/10.1186/s40623-019-1125-4.

Rougier, S., Missenard, Y., Gautheron, C., Barbarand, J., Zeyen, H., Pinna, R., Liégeois, J.P., Bonin, B., Ouabadi, A., Derder, M.E.M., Frizon de Lamotte, D., 2013. Eocene exhumation of the Tuareg Shield (Sahara, Africa). Geology 41, 615–618. https://doi.org/10.1130/G33731.1.

Rubóczki, T., Novák, A., Liptai, N., et al., 2024. The Pannon LitH2Oscope magnetotelluric array in the Pannonian Basin. Acta Geodaetica et Geophysica. https://doi.org/10.1007/s40328-024-00434-1.

Samrock, F., Grayver, A.V., Bachmann, O., Karakas, Z., Saar, M.O., 2021. Integrated magnetotelluric and petrological analysis of felsic magma reservoirs: insights from Ethiopian rift volcanoes. Earth Planet. Sci. Lett. 559. https://doi.org/10.1016/j.epsl.2021.116765. 10.31223/X5Q600.

Schandelmeier, H., Richter, A., Harms, U., 1987. Proterozoic deformation of the East Saharan Craton in Southeast Libya. South Egypt and North Sudan. *Tectonophysics* 140 (2–4), 233–246. https://doi.org/10.1016/0040-1951(87)90231-9.

Schmidt, M.W., 1992. Amphibole Composition in Tonalite as a Function of Pressure: An Experimental Calibration of the Al-in-Hornblende Barometer. Contrib. Mineral. Petrol. 110, 304–310. https://doi.org/10.1007/BF00310745.

Schmincke, H.U., 2004. Continental Intraplate Volcanoes. In: Volcanism. Springer, Berlin, Heidelberg. https://doi.org/10.1007/978-3-642-18952-4_7.

Sebai, A., Stutzmann, E., Montagner, J.P., Sicilia, D., Beucler, E., 2006. Anisotropic structure of the African upper mantle from Rayleigh and Love wave tomography. Phys Earth Planet Inter 155 (1–2), 48–62. https://doi.org/10.1016/j.pepi.2005.09.009.

Sheng, Y., Jin, S., Comeau, M.J., et al., 2021. Lithospheric structure near the northern Xainza-Dinggye Rift, Tibetan Plateau – implications for rheology and tectonic dynamics. J. Geophys. Res. Solid Earth. https://doi.org/10.1029/2020JB021442.

Sheng, Y., Jin, S., Comeau, M.J., Becken, M., Zhang, L., Dong, H., et al., 2022. Controls on the metallogenesis of the Lhasa-Mozugongka district, Gangdese Belt, Tibetan Plateau: Constraints on melt distribution and viscosity from the 3-D electrical structure of the lithosphere. Ore Geol Rev 145. https://doi.org/10.1016/j.oregeorev.2022.104881.

Sheng, Y., Jin, S., Comeau, M.J., Hou, Z., et al., 2023. Evidence for partial melting and alkali-rich fluids in the crust from a 3-D electrical resistivity model in the vicinity of the Coqen region, western Lhasa terrane. Tibetan Plateau. *Earth Planet. Sci. Lett* 619. https://doi.org/10.1016/j.epsl.2023.118316.

Stein, C., Comeau, M.J., Becken, M., Hansen, U., 2022. Numerical study on the style of delamination. Tectonophysics. 827, 229276. https://doi.org/10.1016/j.tecto.2022.229276.

Takherist, D., Lesquer, A., 1989. Mise en évidence d'importantes variations régionales du flux de chaleur en Algérie. Can. J. Earth Sci. 26, 615–626. https://doi.org/10.1139/e89-053.

Tschegg, C., Ntaflos, T., Akinin, V.V., 2011. Polybaric petrogenesis of Neogene alkaline magmas in an extensional tectonic environment: Viliga Volcanic Field, northeast Russia. Lithos 122 (1–2), 13–24. https://doi.org/10.1016/j.lithos.2010.11.009.

Türkoğlu, E., Unsworth, M., Çağlar, İ., Tuncer, V., Avşar, Ü., 2008. Lithospheric structure of the Arabia-Eurasia collision zone in eastern Anatolia: magnetotelluric evidence for widespread weakening by fluids? Geology 36, 619–622. https://doi.org/10.1130/G24683A.1.

Unsworth, M.J., Rondenay, S., 2012. Mapping the distribution of fluids in the crust and lithospheric mantle utilizing geophysical methods. In Metasomatism and the Chemical Transformation of Rock (eds Harlov, D. E., & Austrheim, H.) 535–598 (Springer, Berlin).

Unsworth, M., Comeau, M.J., Diaz, D., Brasse, H., Heit, B., Favetto, A., et al., 2023. Crustal structure of the Lazufre volcanic complex and the southern Puna from 3-D inversion of magnetotelluric data: Implications for surface uplift and evidence for melt storage and hydrothermal fluids. Geosphere 19 (5), 1210–1230. https://doi.org/10.1130/GES02506.1.

Vail, J.R., 1985. Pan African (Late Precambrian) tectonic terrains and the reconstruction of the Arabian-Nubian Shield. Geology 13, 839–842. https://doi.org/10.1130/0091-7613(1985)13<839:PLPTTA>2.0.CO;2.

Wang, T., Ma, G., Comeau, M.J., Becken, M., Zhou, Z., Liu, W., et al., 2022. Evidence for the superposition of tectonic systems in the northern Songliao Block, NE China, revealed by a 3-D electrical resistivity model. J. Geophys. Res. Solid Earth 127 (4). https://doi.org/10.1029/2021JB022827.

Wannamaker, P.E., Hasterok, D.P., Johnston, J.M., Stodt, J.A., Hall, D.B., Sodergren, T. L., Pellerin, L., Maris, V., Doerner, W.M., Groenewold, K.A., Unsworth, M.J., 2008. Lithospheric dismemberment and magmatic processes of the Great Basin-Colorado Plateau transition, Utah, implied from magnetotellurics. Geochem Geophys Geosyst 9. https://doi.org/10.1029/2007GC001886.

Wortel, M.J.R., Spakman, W., 2000. Subduction and slab detachment in the Mediterranean-Carpathian region. Science 290 (5498), 1910–1917. https://doi.org/10.1126/science.290.5498.1910.

Yahiaoui, R., 2003. Étude du volcanisme alcalin de la région de l'Assekrem (Hoggar central). Etude pétrographique, minéralogique, géochimique et géothermobarométrique. USTHB-FSTGAT, Algiers, Algeria, *Thesis*.